AGR Review Meeting, July 13, 2022

Oxidation behavior of silicon carbide and graphitic materials

Haiming Wen[1,2]

[1.] Department of Materials Science and Engineering, Missouri University of Science and Technology

[2.] Department of Nuclear Engineering and Radiation Science, Missouri University of Science and Technology

MISSOURI S&T

Haiming Wen

wenha@mst.edu

NEUP Nuclear Energy University Program

U.S. Department of Energy

TRISO coated fuel particles

- TRISO coated particles designed for high temperature gas reactor (HTGR)
- ~0.5 to 0.9 mm sphere
- Fuel kernel for TRISO particles: UO_2 or UCO
- TRISO coating: carbon buffer layer, inner PyC layer, SiC layer, outer PyC layer
- SiC layer: principal structural layer and primary barrier for fission product transport
- Particles act as small pressure vessels
- Fission products remain inside coatings

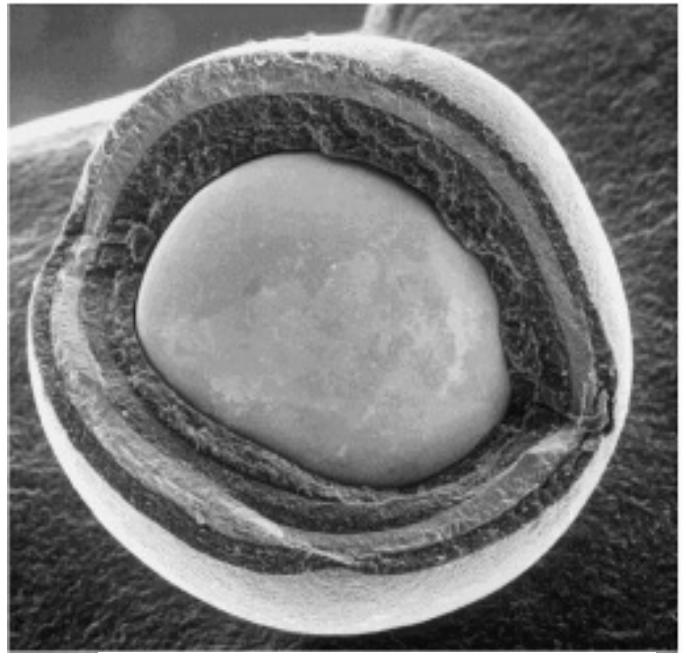

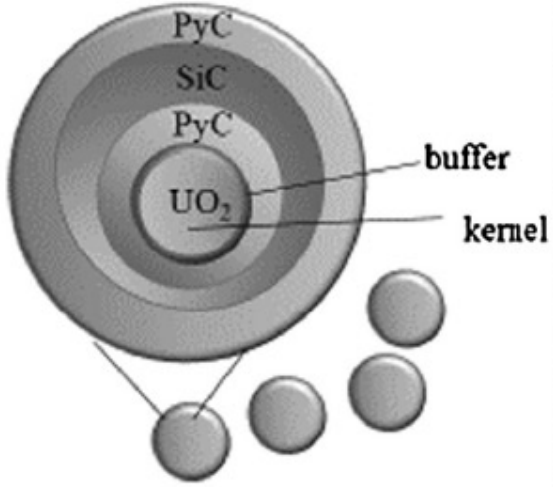

TRISO particles

TRISO Fuel: Prismatic Fuel System

- TRISO fuel particles pressed into compacts with graphitic matrix
- Fuel assembly has channels for fuel compacts and channels for gas (coolant) flow

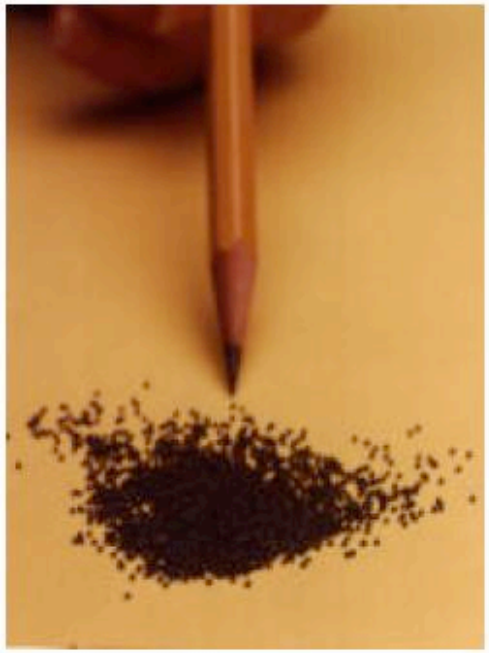

TRISO Coated Particles →

Compacts →

Fuel Assembly

TRISO Fuel: Pebble Bed Modular Reactor

- Fuel element for the Pebble Bed Modular Reactor
- 11,000 TRISO particles in every pebble

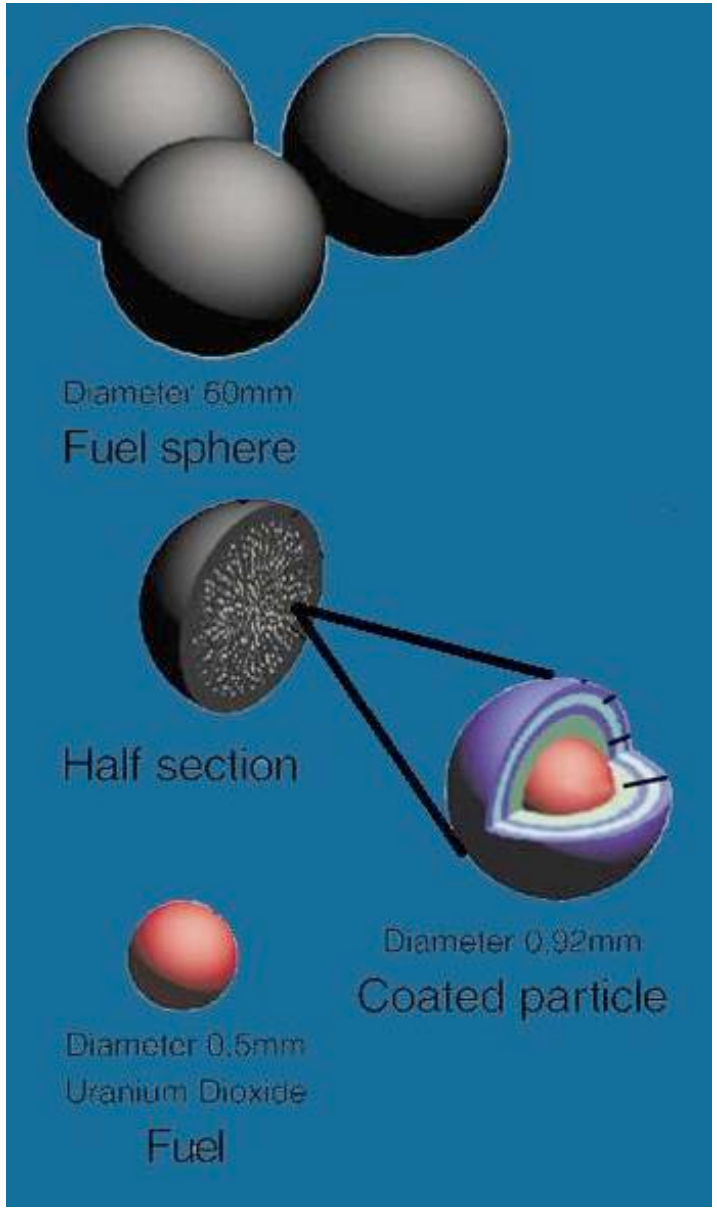

Air Ingress Events in HTGRs

- Air-ingress:
  - ➢Break of primary coolant pipe
  - ➢Reactor coolant system depressurization
  - ➢Air entrance and natural circulation within system

Maximum Fuel Temperature (°C)	1600 +
Total air pressure (kPa)	101.3
O_2 partial pressure (kPa)	~ 0 to 21
Total Duration (hours)	100 +

Preliminary Safety Information Document for the Standard MHTGR, Vol. 1, HTGR-86-024 (1986).

Oxidation of graphite in air

Primary mechanism which has lowest energy is

$$C + xO_2 \rightarrow zCO \ (\Delta H = -391 \text{ kJ/mol})$$

Temperature Regimes: oxidation kinetics have three distinct temperature regimes.

- Regime I: Chemical diffusion throughout matrix
- Regime II: Some chemical diffusion through matrix and transport through pores
- Regime III: only surface layer is oxidized, diffusion controlled

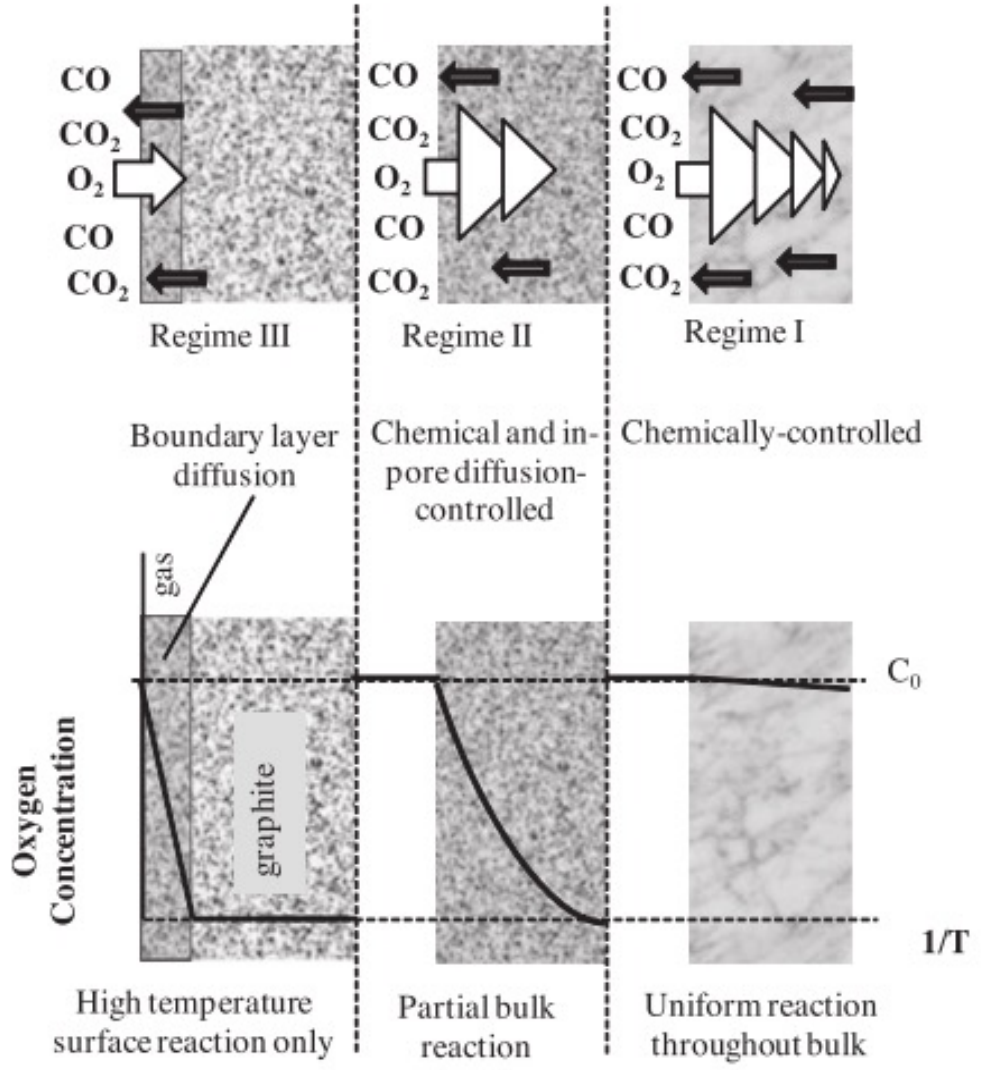

Fig. 1. Oxidation modes of porous nuclear-grade graphite from Regimes I to III.

J.J. Lee, T.K. Ghosh, S.K. Loyalka, J. Nucl. Mater. 438 (2013) 78–87.

Matrix-Grade Graphite: A3-3 & A3-27

Similarities

- Composition: ~64% natural graphite; ~16% electro-graphite; ~20% phenol resin binder
- Fed into hopper mill to achieve desired grain size
- Cold Pressed to shape
- Heat treatment at 1800-1950°C

Differences

Grade	Binder Composition	Binder Fabrication	Binder Properties
A3-3 (RDKRS)	Phenol-formaldehyde	Dissolved in alcohol, then added to matrix powders	2D cross-linkage Thermoplastic
A3-27 (ARB-B1)	Phenol-hexamethylenetetramine	Mixed with powders and synthesized during matrix formation	3D cross-linkage Thermoset

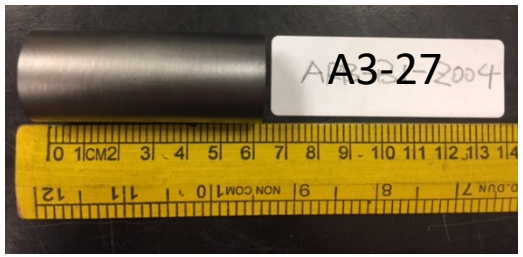

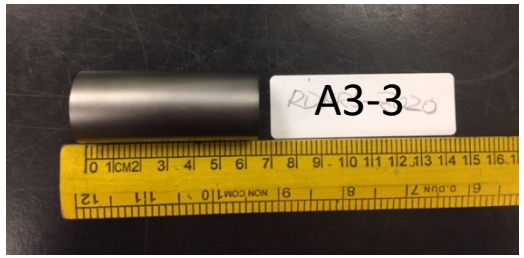

Verfondern, Karl, et al. *High-Quality Thorium TRISO Fuel Performance in HTGRs*. Forschungszentrum Jülich, 2013.

TEM: Matrix Graphite

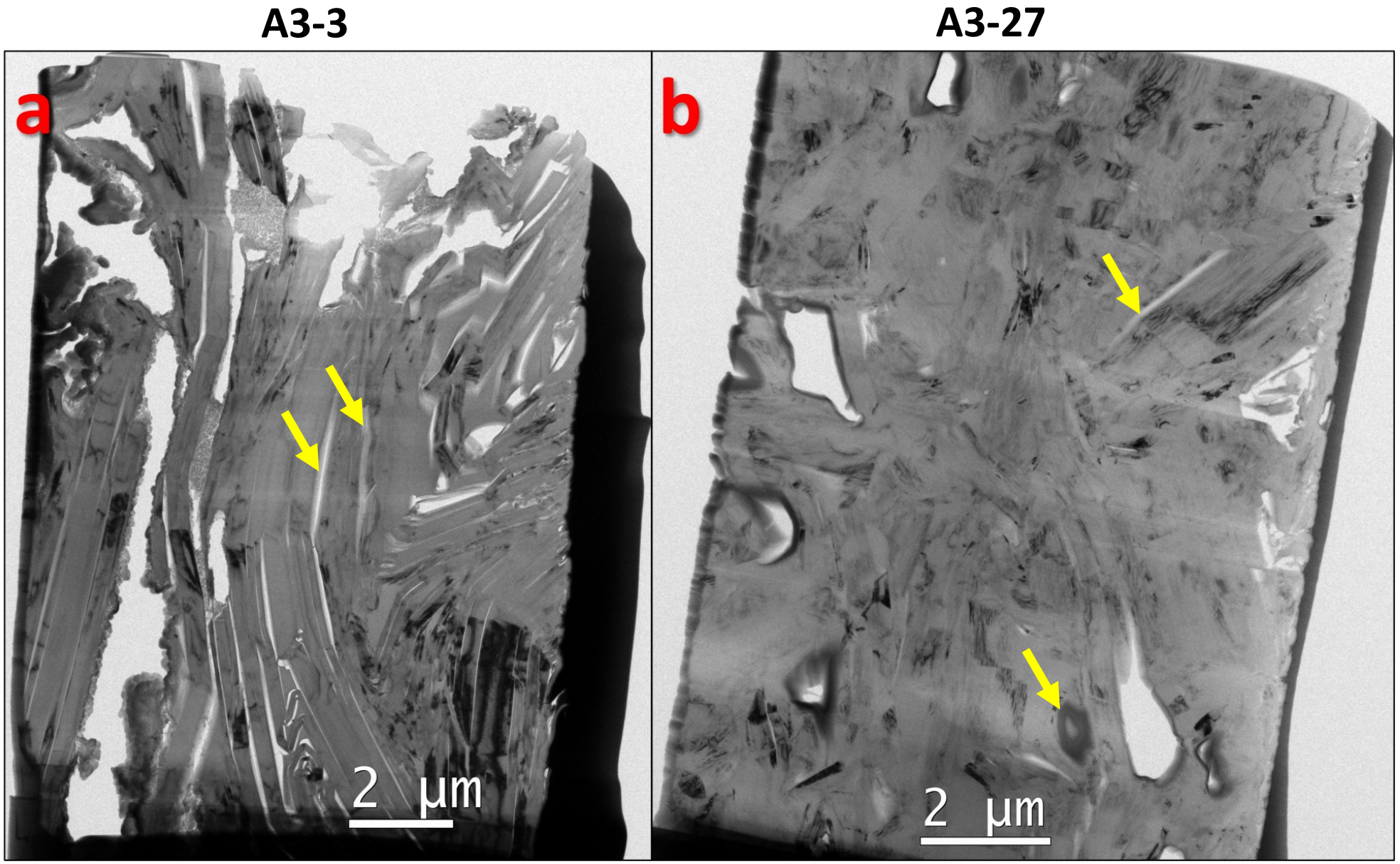

- The grains and partially graphitic regions observed in A3-3 matrix graphite are generally elongated
- The features in A3-27 are more isotropic or rounded

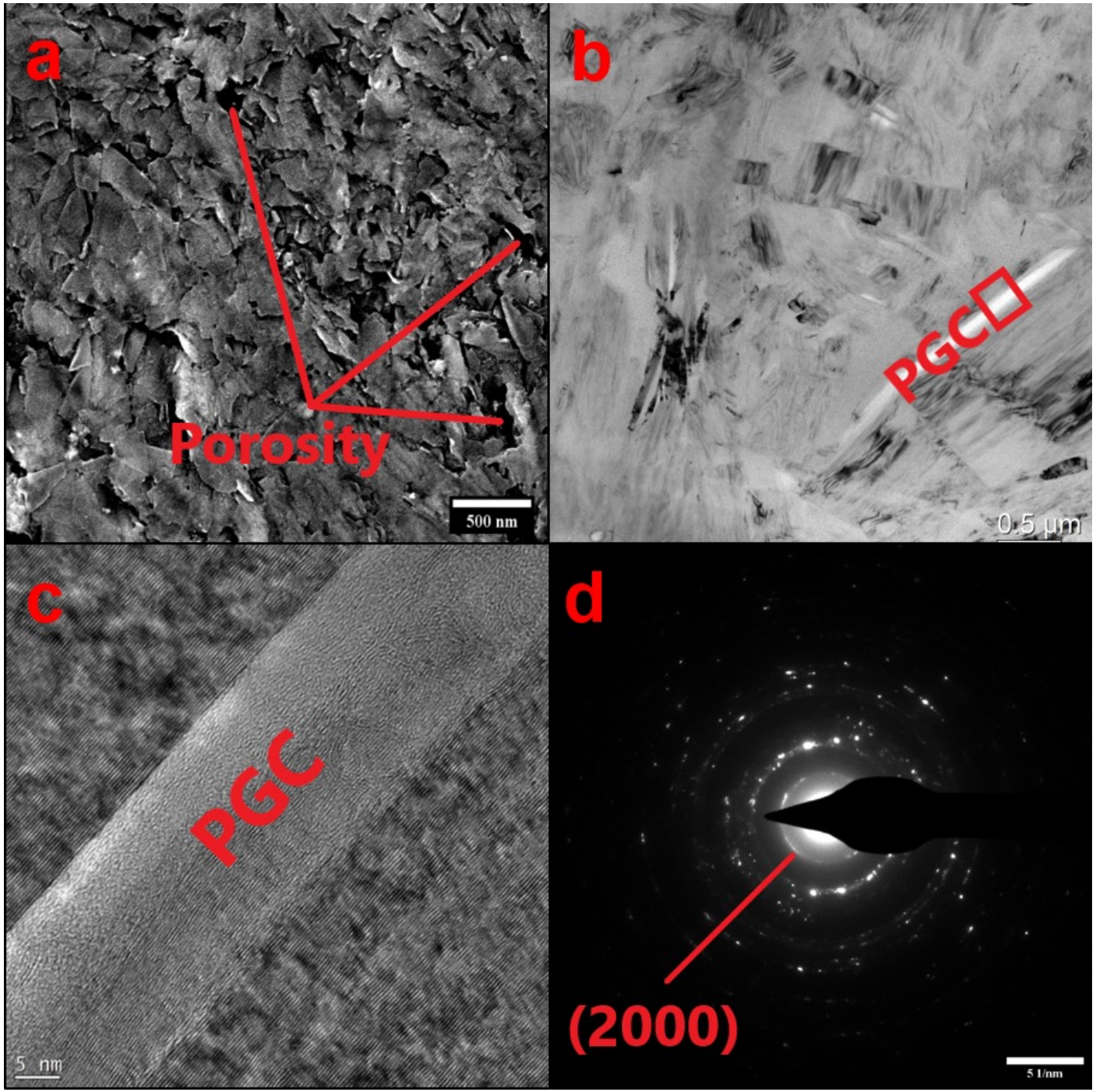

Electron microscopy: A3-27 matrix graphite

- Characterized via SEM, TEM, HR-TEM, and SAED
- SAED suggests relatively random grain orientation, which is also supported by the BF-TEM in (b)
- HR-TEM shows partially graphitized carbon (PGC) between graphitic grains

Bratten AT, Wen HM, et al., "Effects of Microstructure on the Oxidation Behavior of A3 Matrix-Grade Graphite", *Journal of the American Ceramic Society* 104 (2021) 584-592.

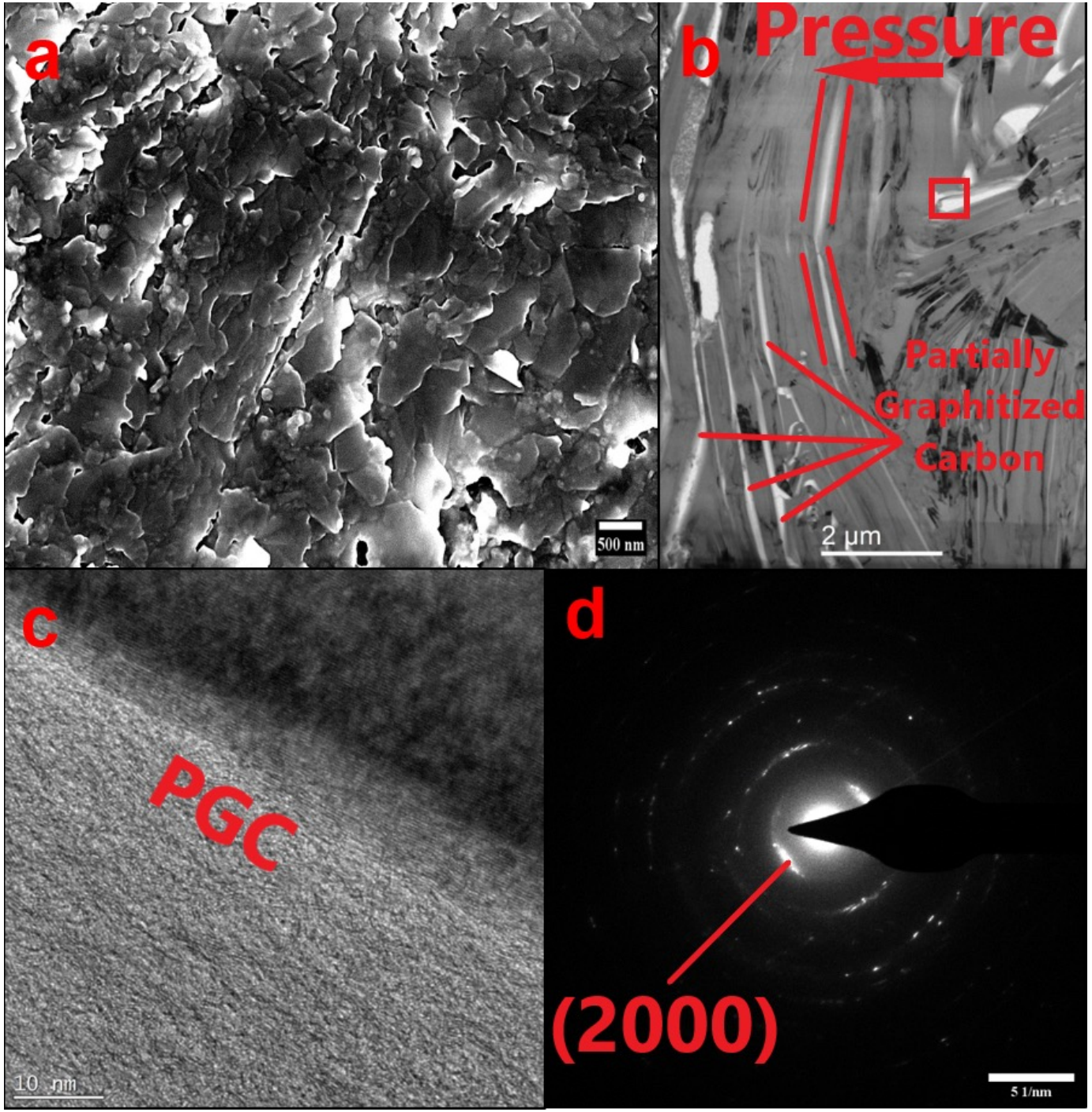

Electron microscopy: A3-3 matrix graphite

- Features are more directionally aligned (stacked sheets)
- Apparently greater PGC content
- Possibly more disorder in PGC than that in A3-27
- Greater anisotropy in SAED than A3-27

Bratten AT, Wen HM, et al., "Effects of Microstructure on the Oxidation Behavior of A3 Matrix-Grade Graphite", *Journal of the American Ceramic Society* 104 (2021) 584-592.

Raman: Matrix graphite

1331 → D (disordered) peak
1557 → G (graphite) peak

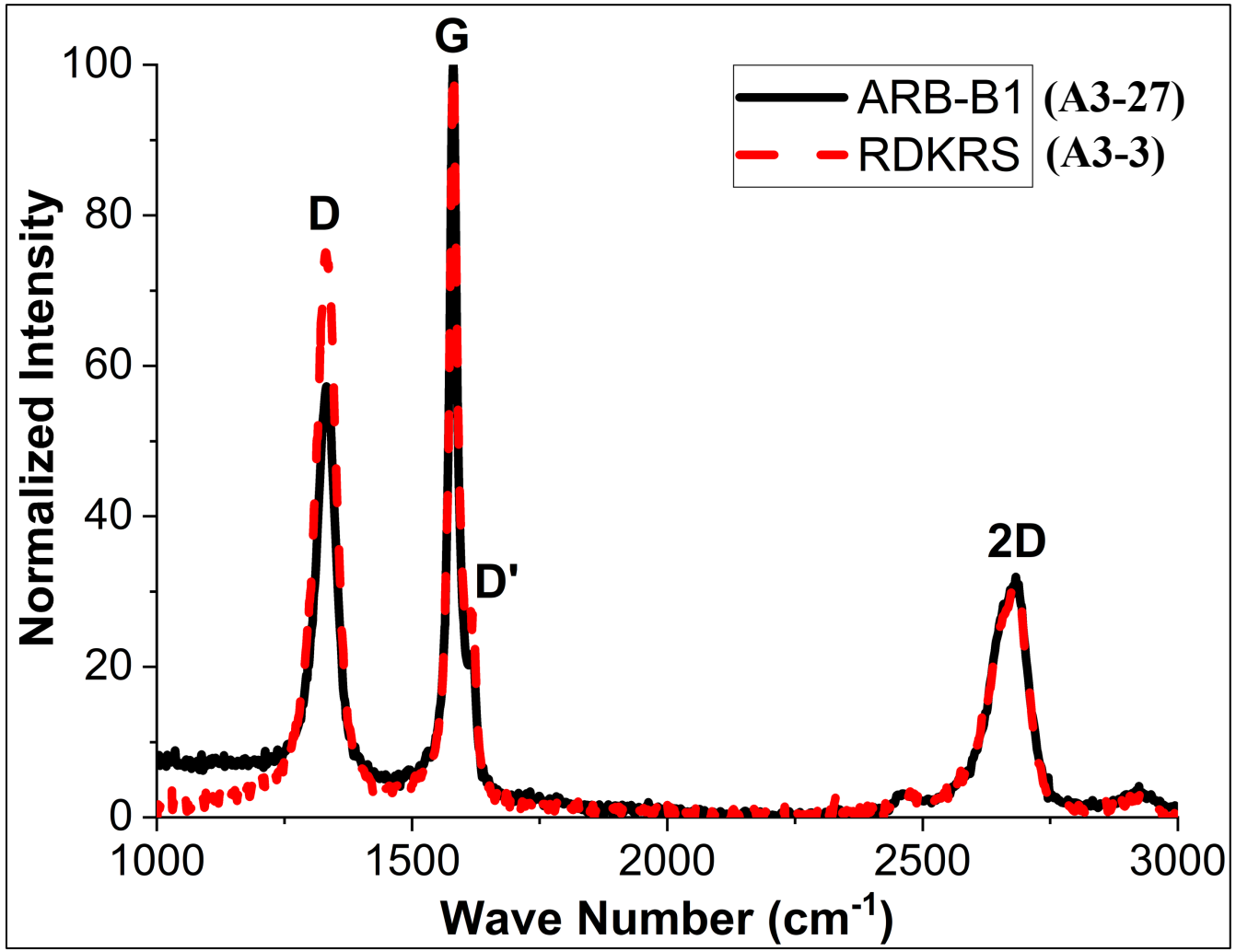

- D-peaks are associated with partially graphitized carbon (binder)
  - Higher-order D peaks at 1620 and 2687 cm^{-1}
- Degree of graphitization compared using a ratio of intensities for D and G peaks
  - A3-3 ID/IG: 0.751
  - A3-27 ID/IG: 0.571
- A3-3 type matrix graphite contains more disordered carbon

Electron Energy Loss Spectroscopy (EELS): Matrix Graphite

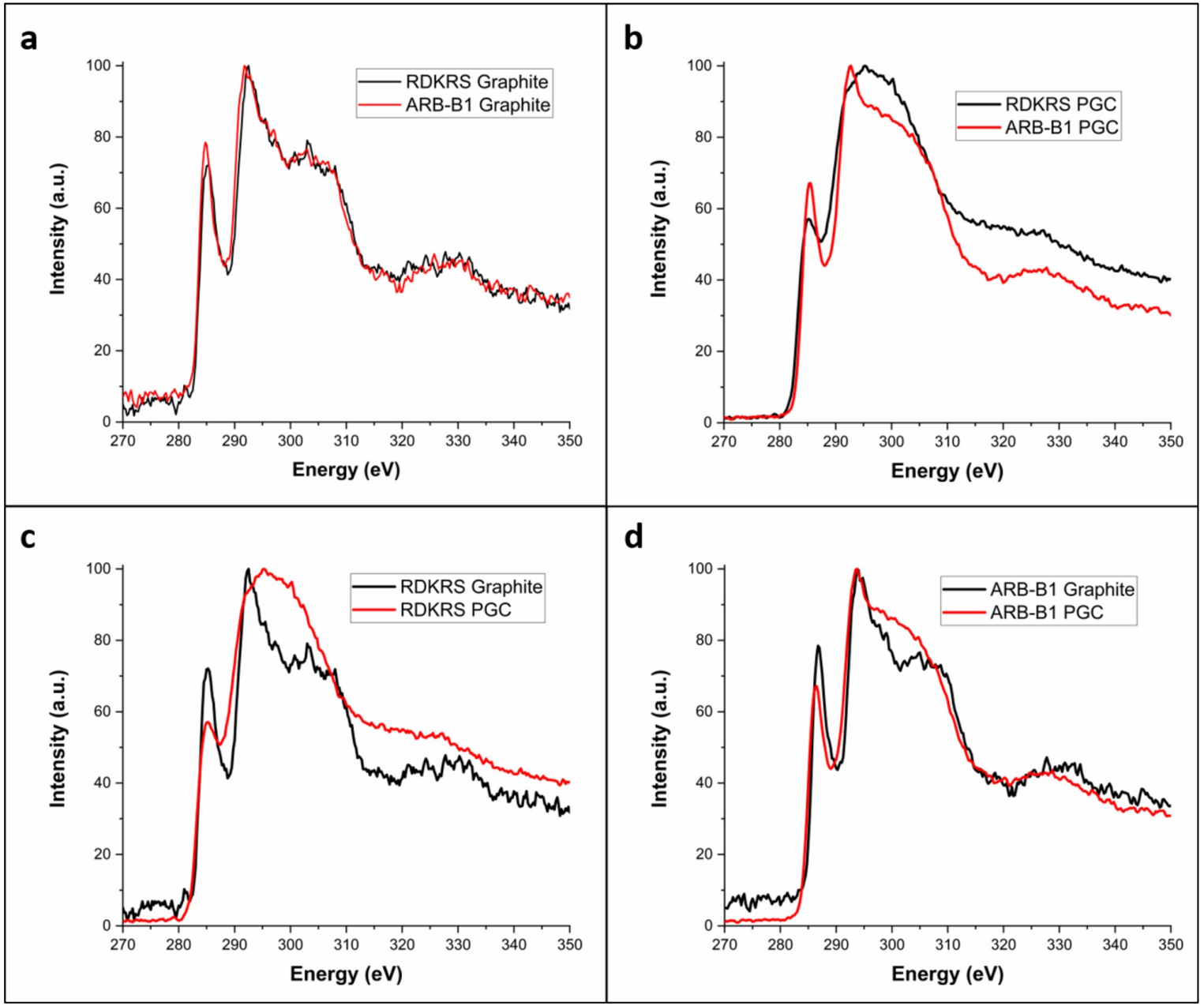

- Graphite in both grades is nearly identical
- PGC structure is different between grades
- PGC is distinct from graphite in both grades
- The difference between PGC and graphite is larger in A3-3 than that in A3-27, suggesting higher degree of disorder for PGC in A3-3 compared to that in A3-27

TGA Analysis in Air: Matrix Graphite

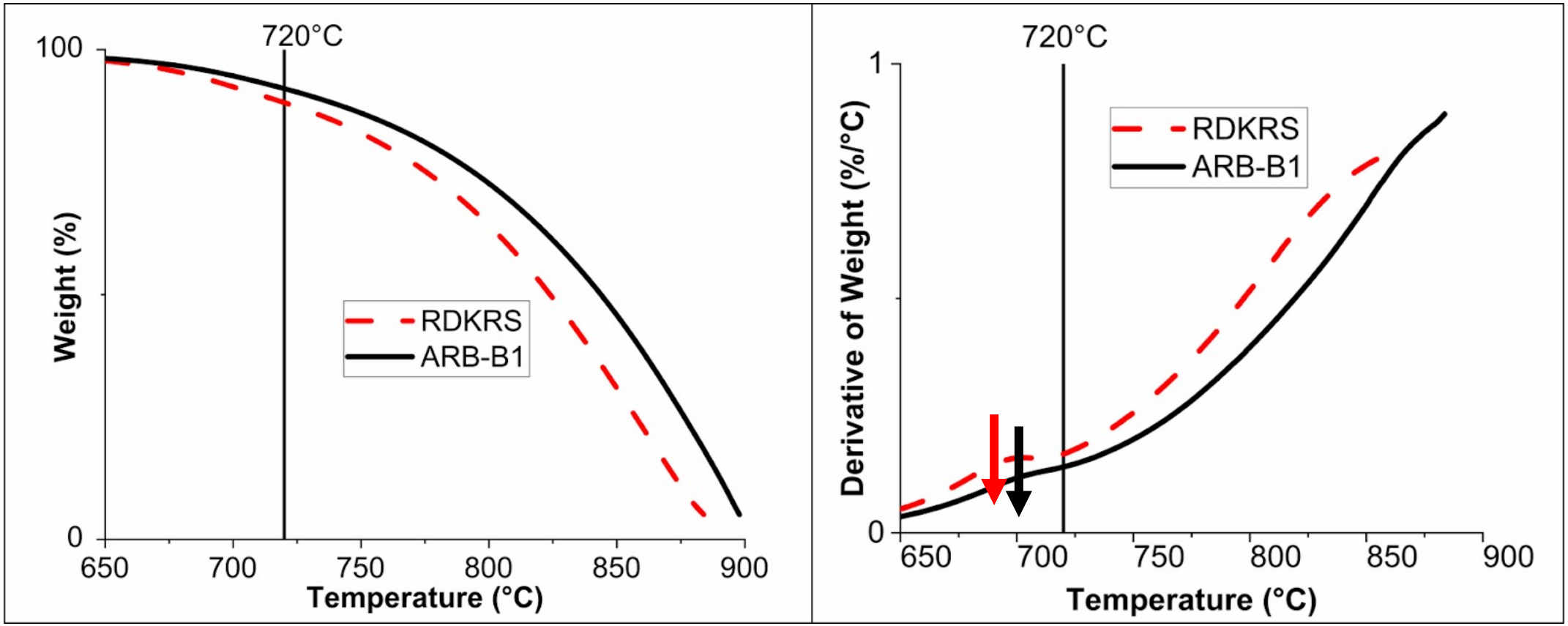

- A3-3 has higher weight loss percentage than A3-27 at the same temperature
- At ~685 °C, a peak in PGC oxidation rate; the PGC oxidation peak was more pronounced for A3-3 than A3-27
- Above ~700 °C, Regime I oxidation of graphite dominates
- At ~720 °C, a transition from Regime I to Regime II oxidation of graphite

DSC Analysis in Air: Matrix Graphite

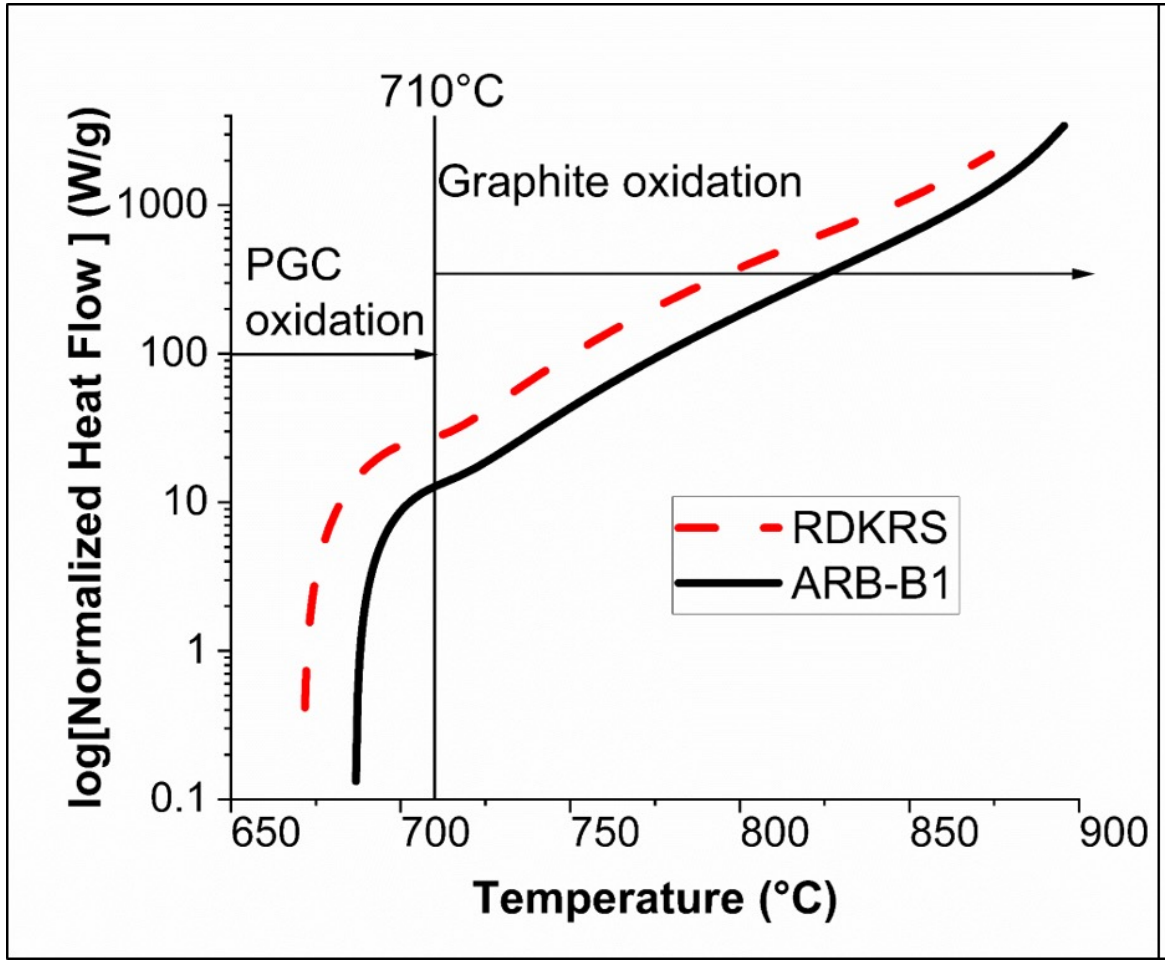

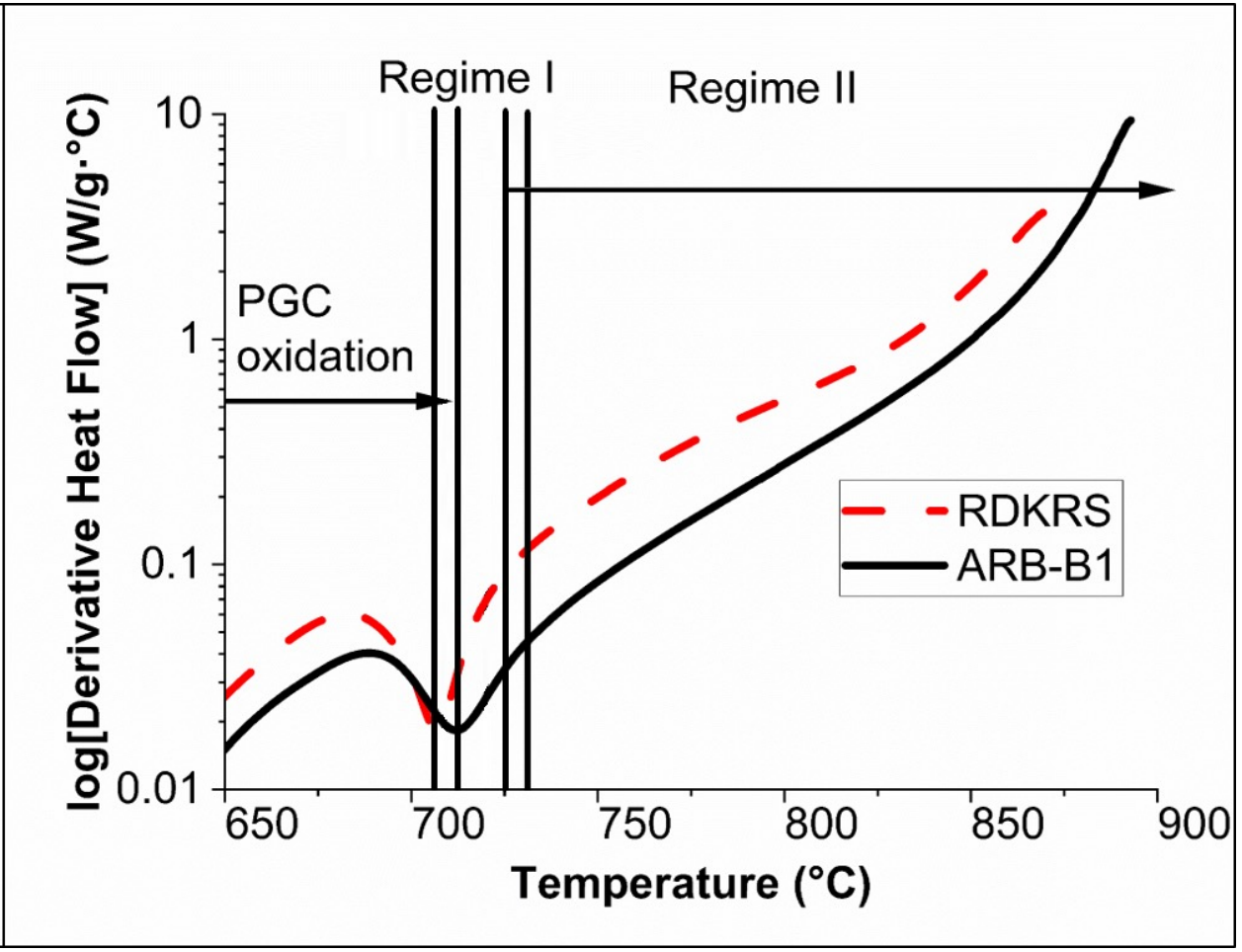

- A3-3 exhibited greater heat flow at all oxidation temperatures
- At ~685 °C, a peak in PGC oxidation rate
- At ~710 °C, a transition from PGC oxidation to graphite oxidation; this transition occurred at a lower temperature for A3-3 than A3-27
- At ~720 °C, a transition from Regime I to Regime II oxidation of graphite; Regime I and Regime II refer to chemical reaction controlled and mixed control oxidation regimes.

Summary: Matrix Graphite Oxidation in Air

- A3-3 type matrix graphite is more directionally-aligned than A3-27 type
- A greater fraction of PGC in A3-3 type matrix graphite than in A3-27 type
- PGC in A3-3 is more disordered than that in A3-27
- A3-3 type oxidized and transitioned from PGC oxidation to graphite oxidation at lower temperatures
- The different fabrication processes (binder type and mixing step) yielded different microstructures, which resulted in different oxidation behavior.
- The 3D cross-linking binder used in A3-27 type produced a more isotropic microstructure and may have converted more uniformly to graphite than the 2D cross-linking binder

Oxidation of SiC in oxygen

- **Two oxidation mechanisms**
  - **Passive oxidation:** at low temperature and high oxygen partial pressure

$$\boldsymbol{SiC_{(s)} + \frac{3}{2} O_{2(g)} \rightarrow SiO_{2(s)} + CO_{(g)}}$$

    - Deal-Grove oxidation behavior: $x^2 + Ax = Bt$

    Where x=oxide layer thickness, B = parabolic rate constant, B/A = linear rate constant

    - Arrhenius dependence: $B = B_0 \exp\left(\frac{-Q}{RT}\right)$

  - **Active oxidation:** at high temperature and low oxygen partial pressure

$$\boldsymbol{SiC_{(s)} + O_{2(g)} \rightarrow SiO_{(g)} + CO_{(g)}}$$

Objective: Measure the oxidation rates of SiC layer of surrogate TRISO fuel particles and determine oxidation mechanisms

Comparison: TRISO Particle Extended Oxidation in Air

- Oxide film remained continuous up to 120 hours at 1000 °C. Pores formed but not cracks.
- Enlarged pores and cracking present at 1100 °C

Cross section made by FIB trenching

Top: 1000 °C
Bottom: 1100 °C

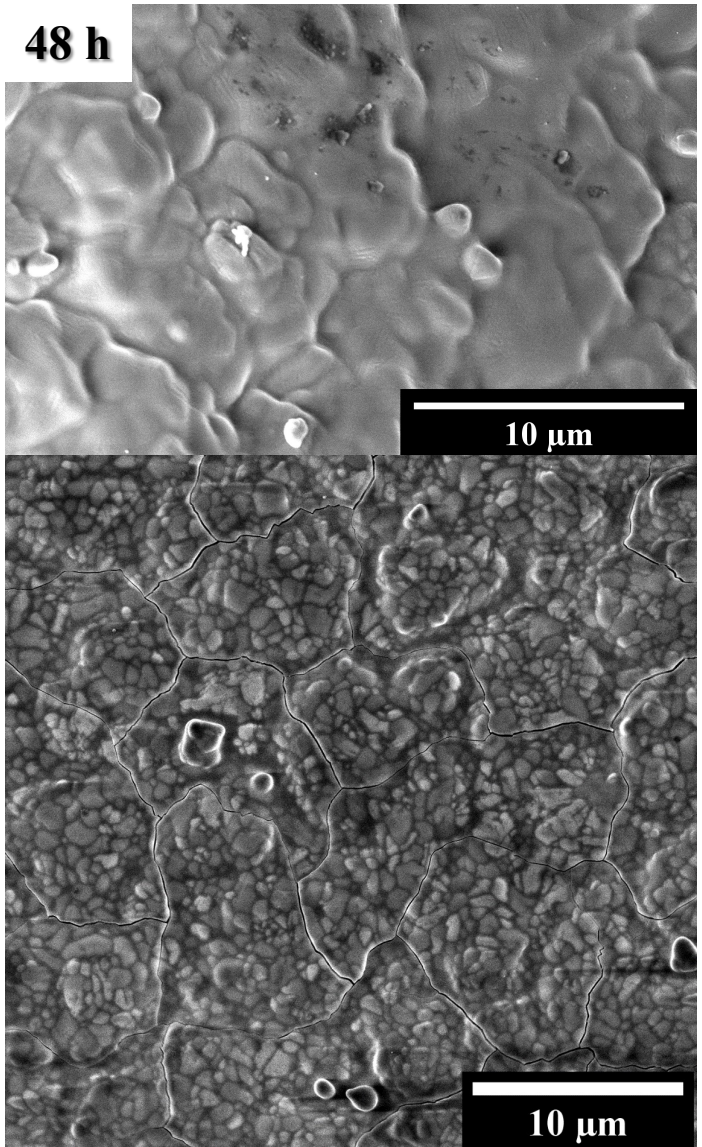

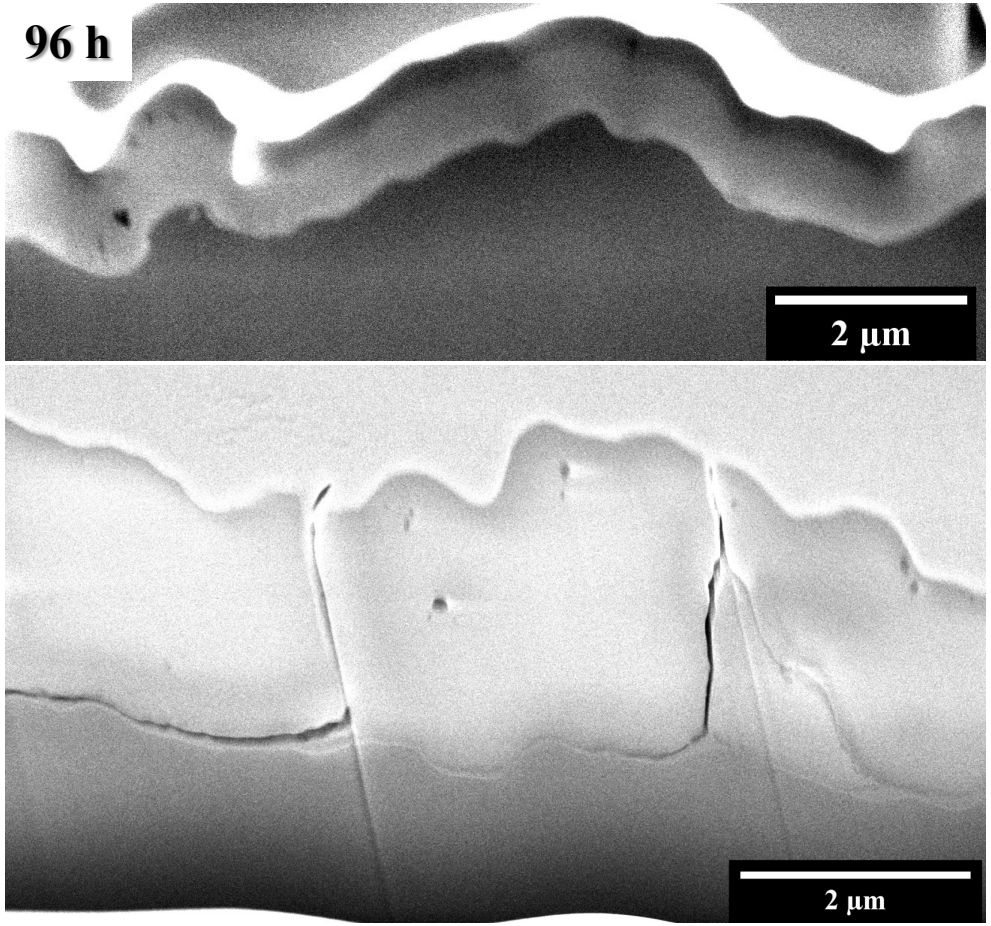

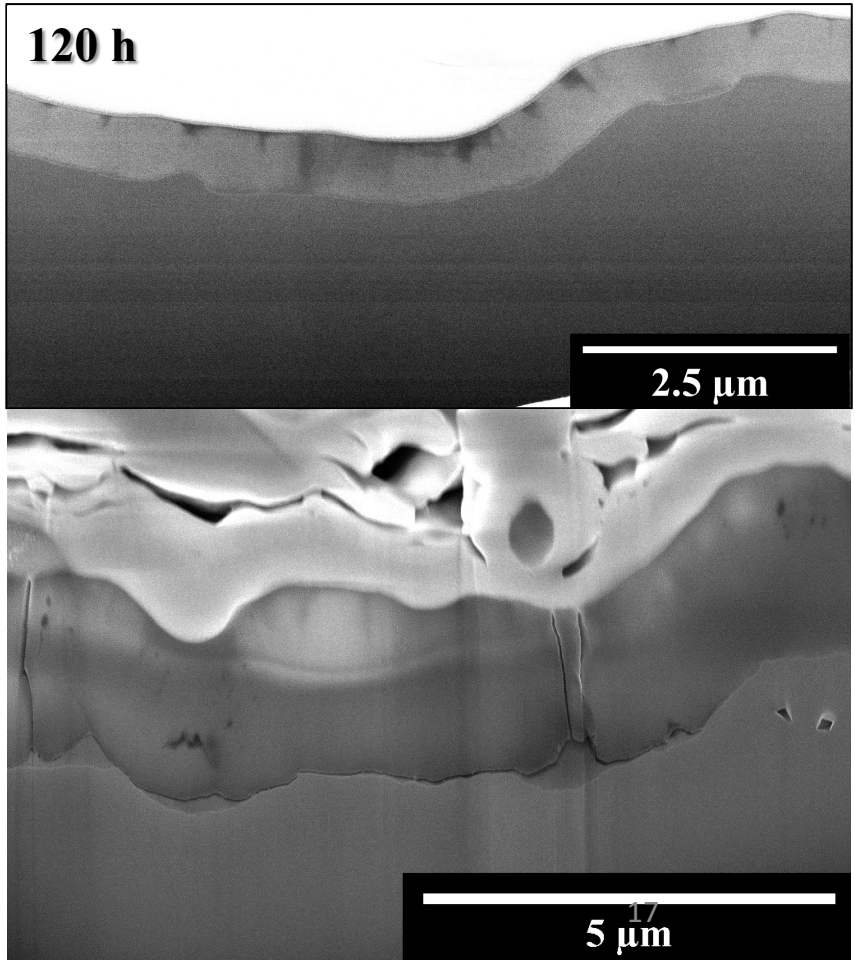

AFM: 1000 °C Oxidized TRISO Particles

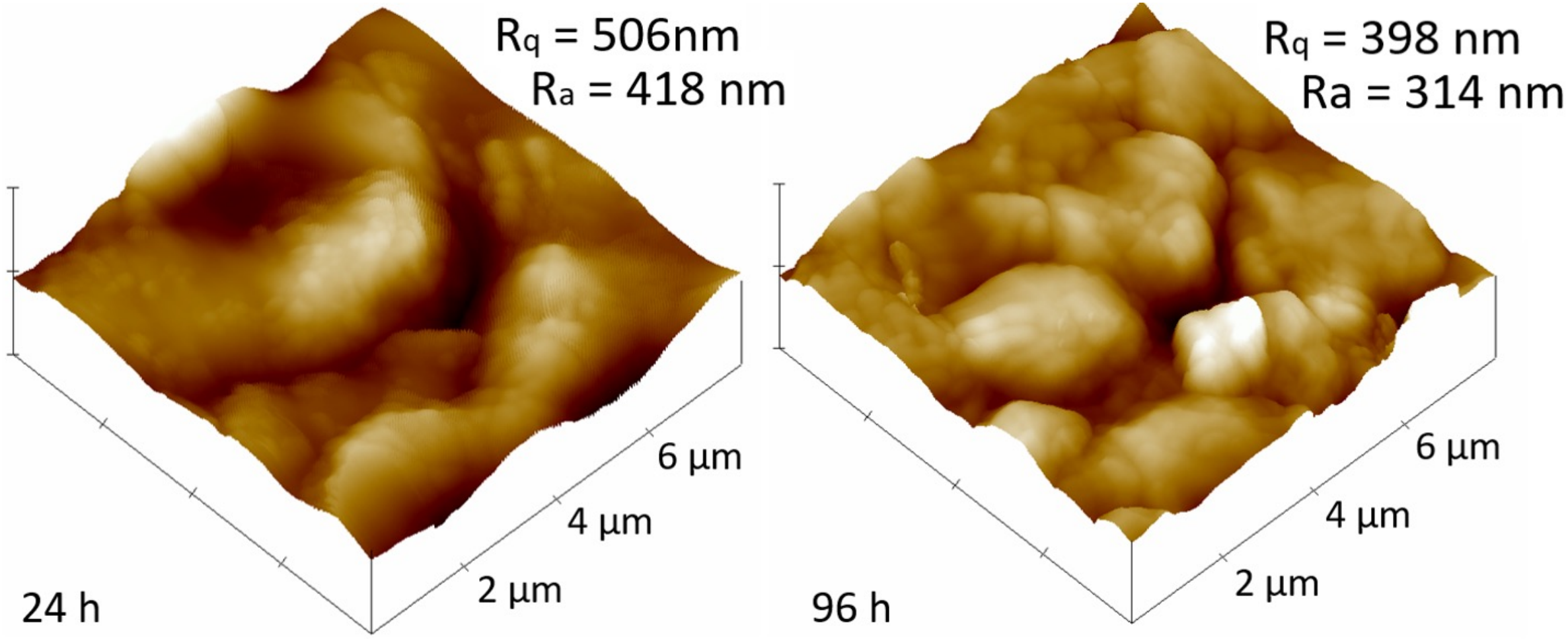

- Roughness was reduced over time, suggesting smoothing of the amorphous oxide film
- Roughness of 1100C samples too great to measure with our AFM

Bratten AT, Wen HM, et al., "Oxide Evolution on the SiC Layer of TRISO Particles during Extended Air Oxidation", *Journal of Nuclear Materials* 558 (2022) 153385.

Oxidation Kinetics in Static Air

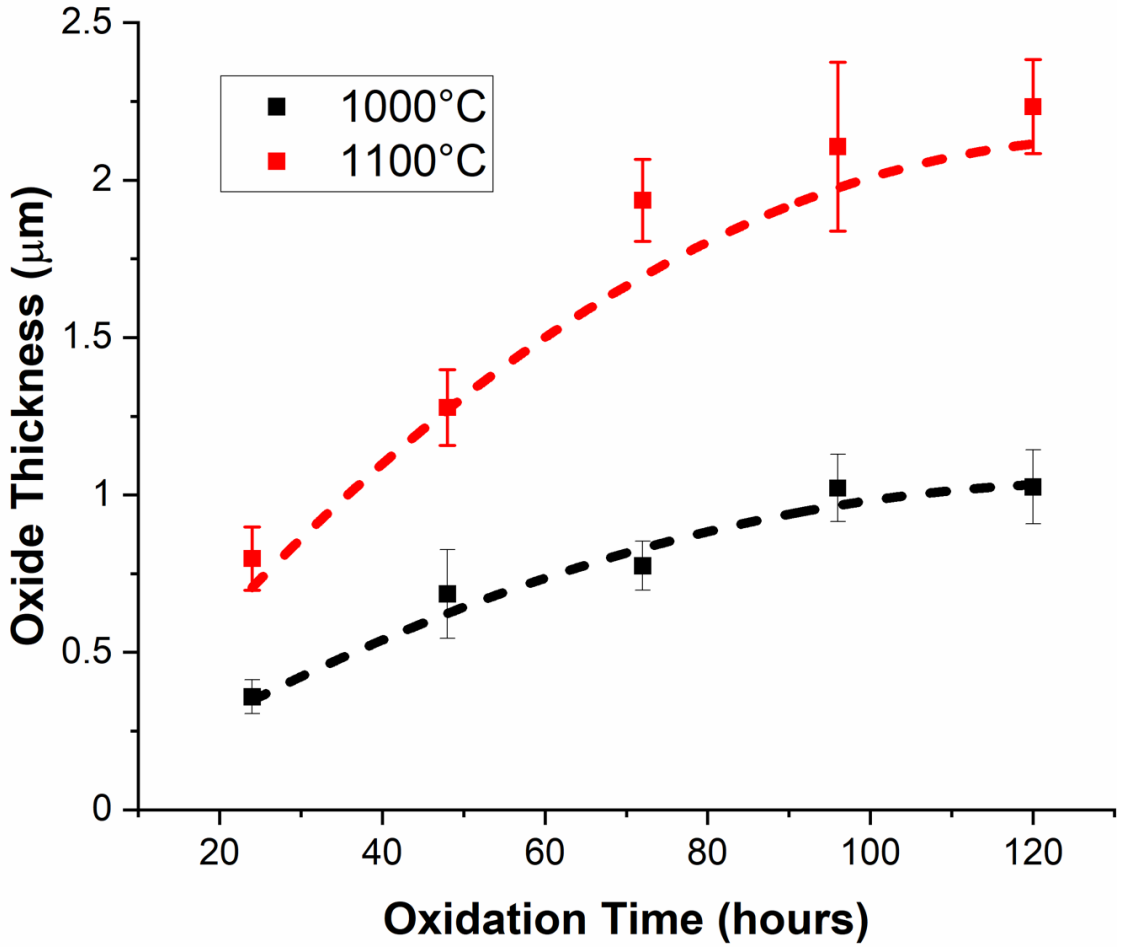

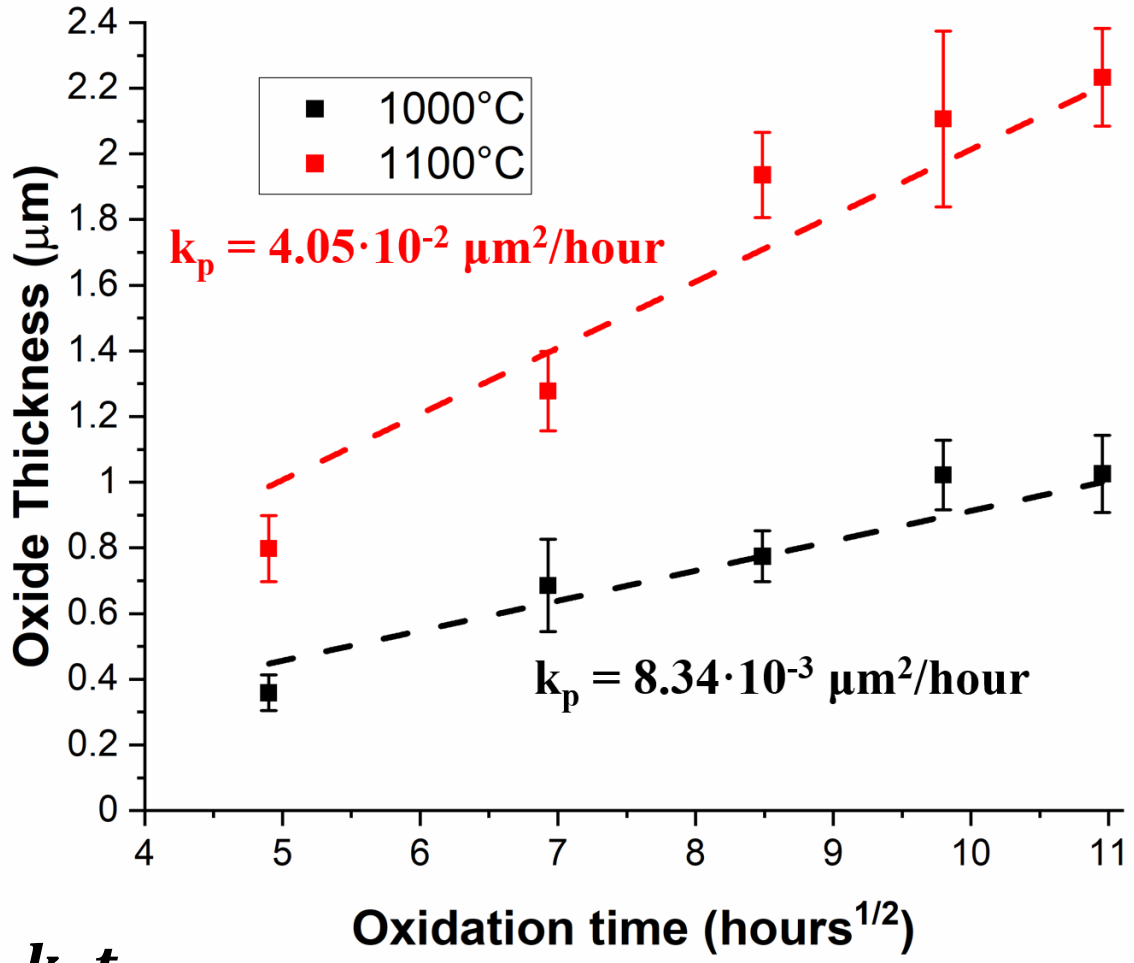

$$x^2 = k_p t$$

- Oxide thickness approximated using parabolic rate law (neglecting the linear stage)
- k_p at 1100 °C was 80% greater than at 1000 °C

Bratten AT, Wen HM, et al., "Oxide Evolution on the SiC Layer of TRISO Particles during Extended Air Oxidation ", *Journal of Nuclear Materials* 558 (2022) 153385.

Oxidation in Flowing 20 kPa O_2 at 1600 °C

- Two regions: deformed (spherulitic) and pristine (amorphous)
- Spherulitic cracks from devitrification of SiO_2
- No significant variations in oxide thickness across the spherulitic region; no porosity

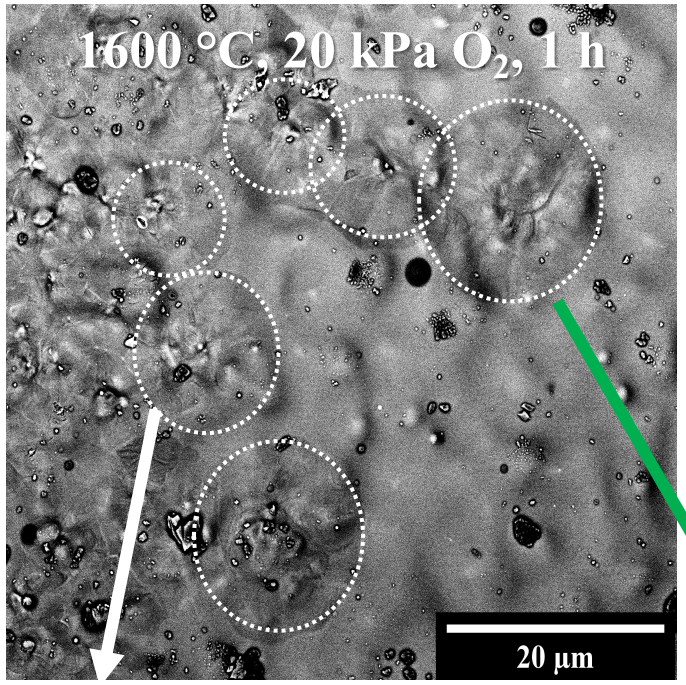

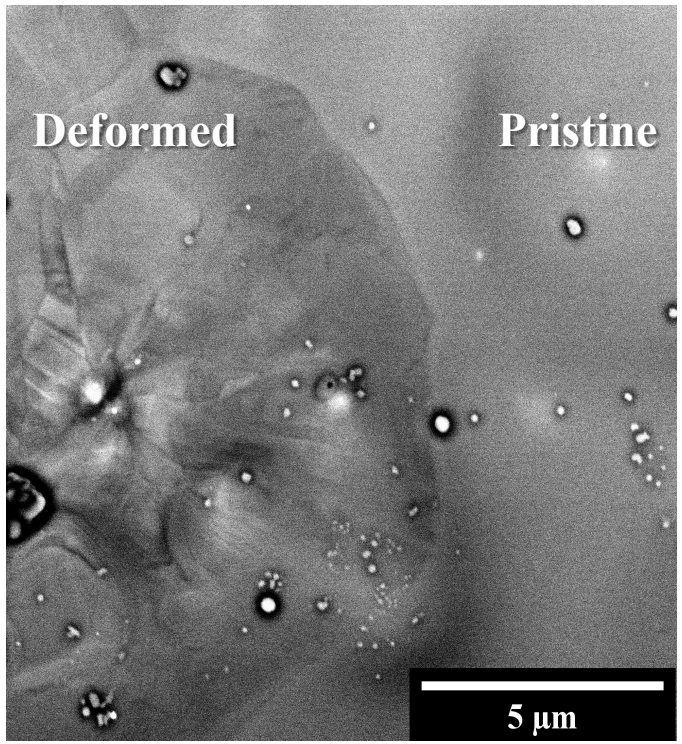

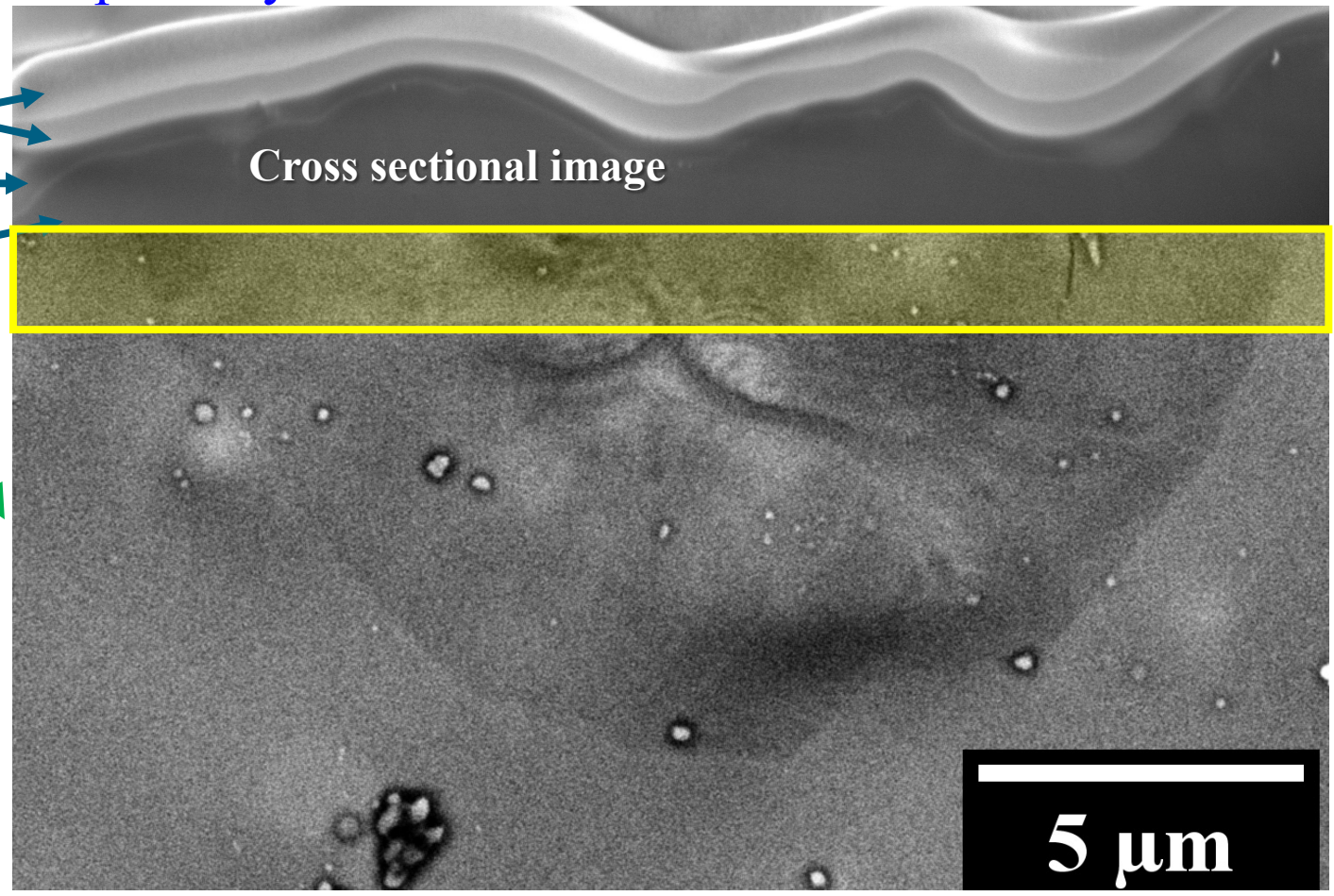

Oxidation in 0.2 kPa O_2

- Raised nodules on surface
- Number density increase with oxidation temperature
- Oxide thickness and interfacial pores near nodules larger than far from nodules

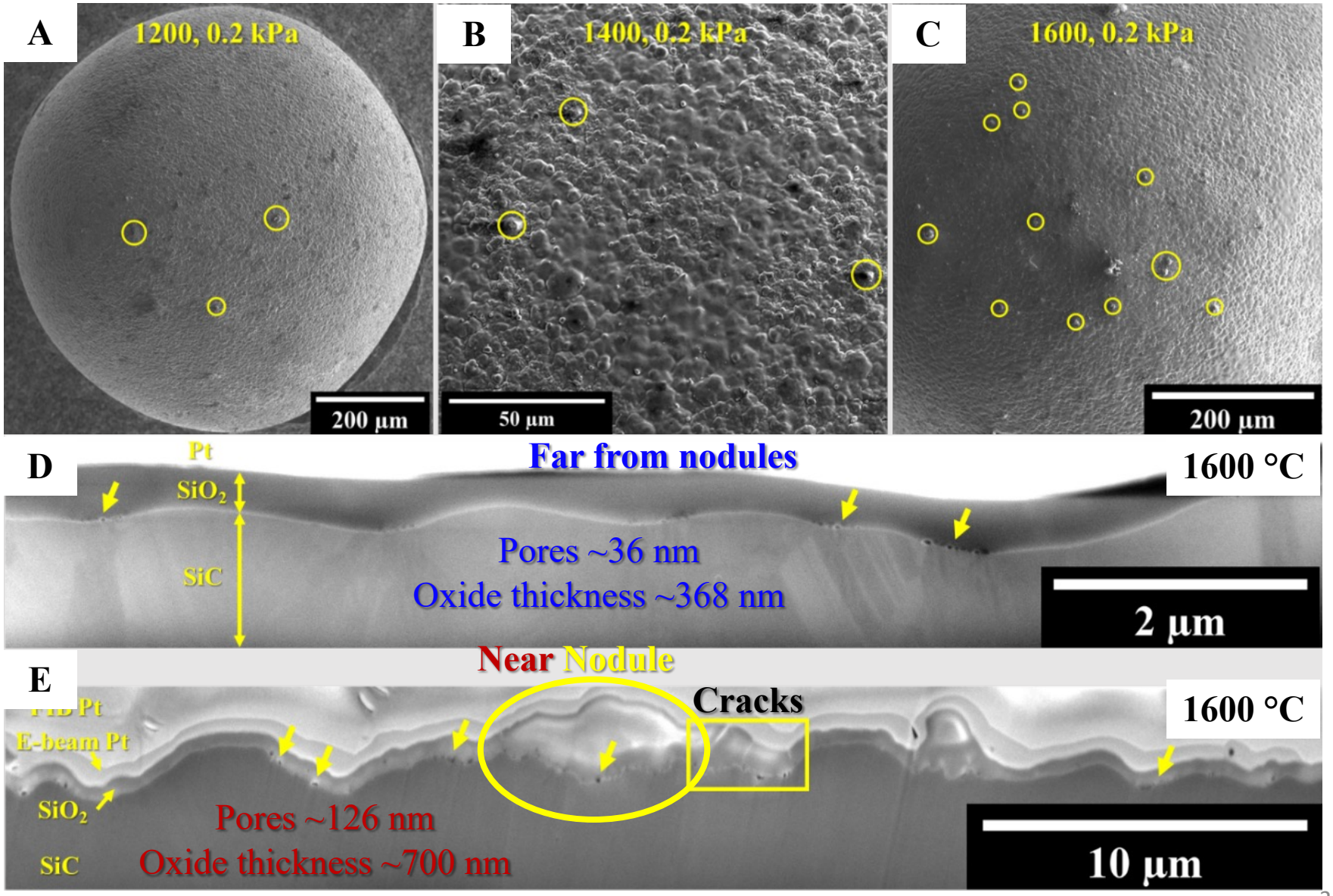

Bratten AT, Wen HM, et al., "High-Temperature Oxidation Behavior of the SiC Layer of TRISO Particles in Low-Pressure Oxygen", submitted to *Journal of Nuclear Materials*.

Nodules formed in 0.2 kPa O_2

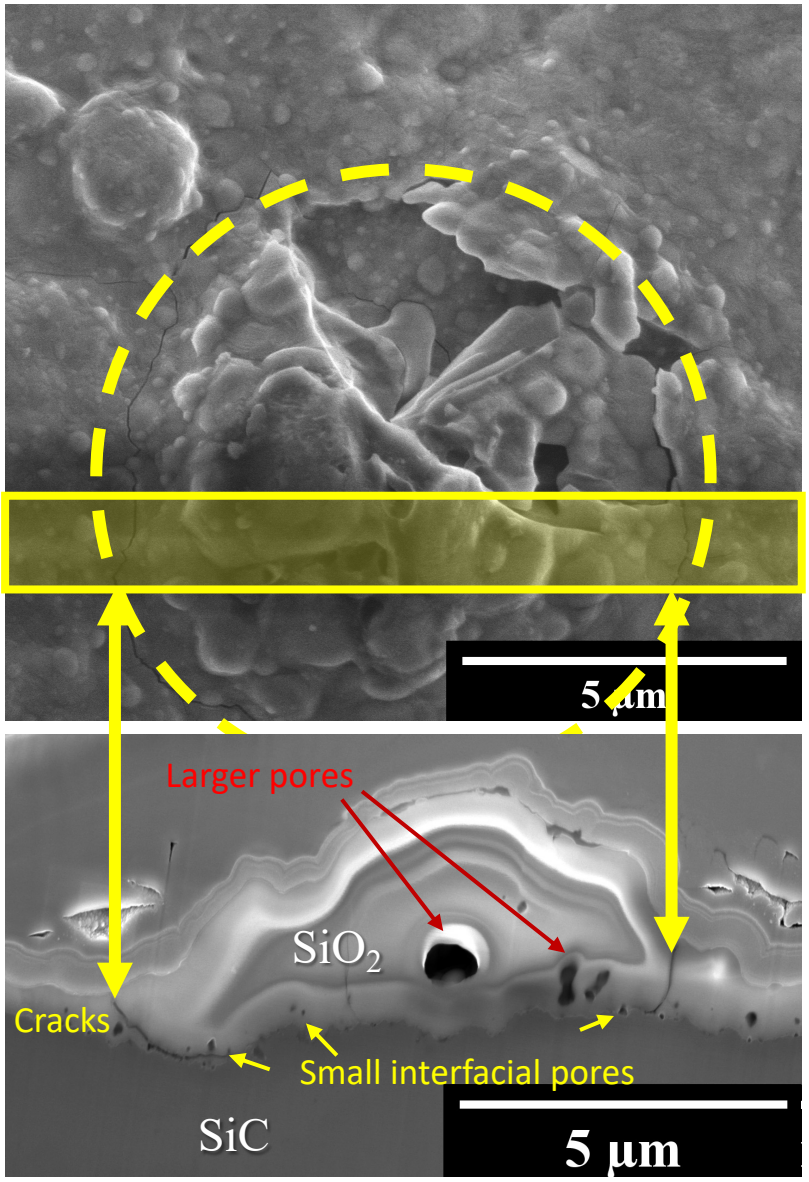

- EDS to rule out surface contamination
- Nodule is pure SiO_2
- Significant porosity and cracking in cross-section
- Cracks in a ring around nodules

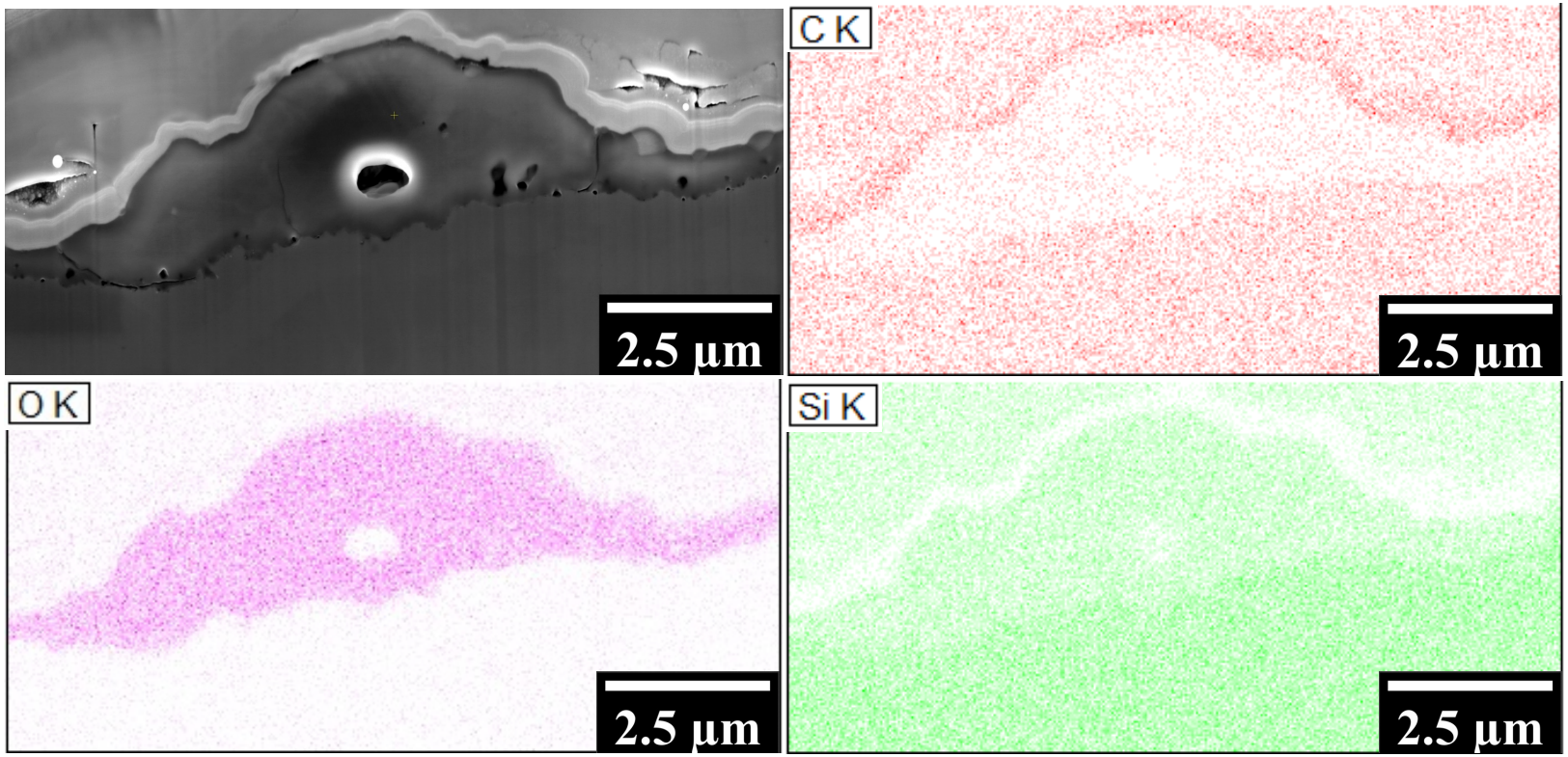

Oxide Growth in 0.2 and 20 kPa O_2

- Oxide growth rate calculated from thickness and oxidation time assuming parabolic rate
  At high temperature, linear stage of oxidation negligible

$$x^2 + Ax = Bt \quad \text{simplified to} \quad x^2 = Bt$$

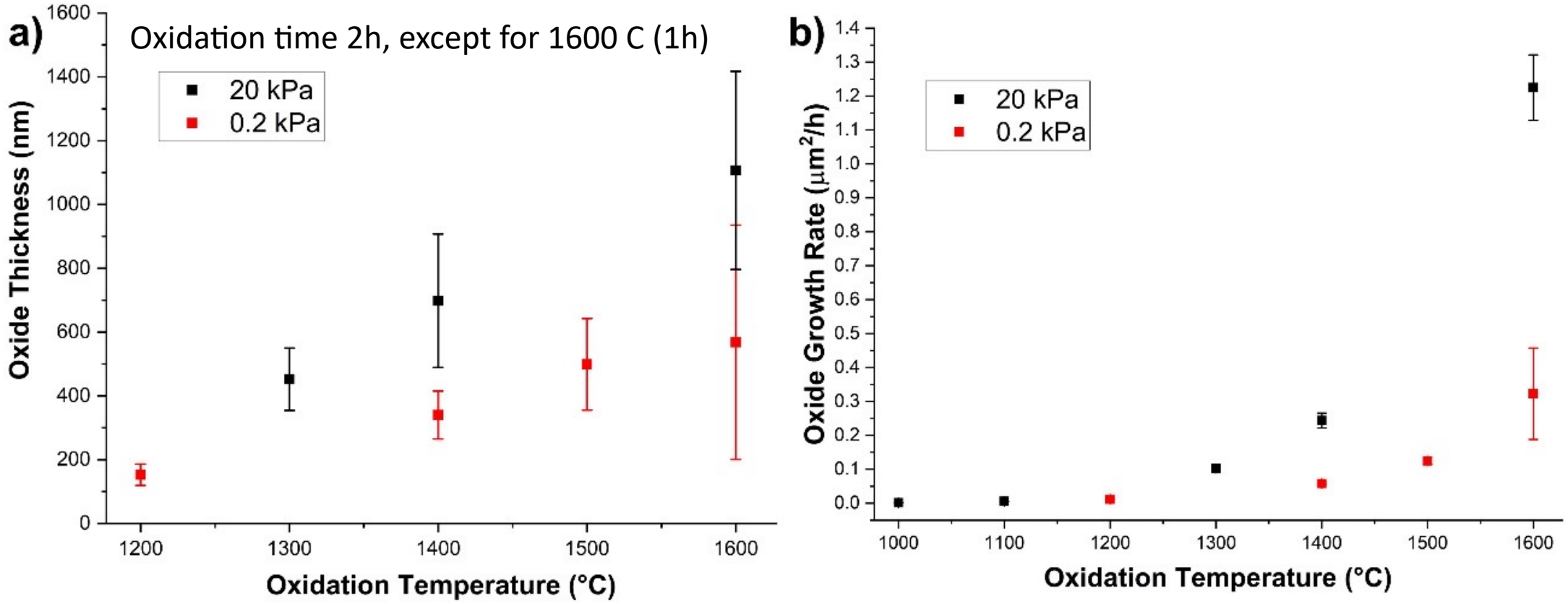

Bratten AT, Wen HM, et al., "High-Temperature Oxidation Behavior of the SiC Layer of TRISO Particles in Low-Pressure Oxygen", submitted to *Journal of Nuclear Materials*.

Oxidation Kinetics in O_2 Environments

- Oxide growth mechanisms consistent across all temperatures; different at 20 kPa vs 0.2 kPa O_2
  - Passive oxidation at 20 kPa O_2 from 1000 – 1600 °C
  - Passive oxidation, as well as active oxidation + redeposition by $SiO_{(g)} + \frac{1}{2}O_{2(g)} \rightarrow SiO_{2(s)}$ at 0.2 kPa O_2 from 1200 – 1600 °C
- Change in oxide growth mechanism between 0.2 and 6 kPa O_2 based on pO_2 dependence

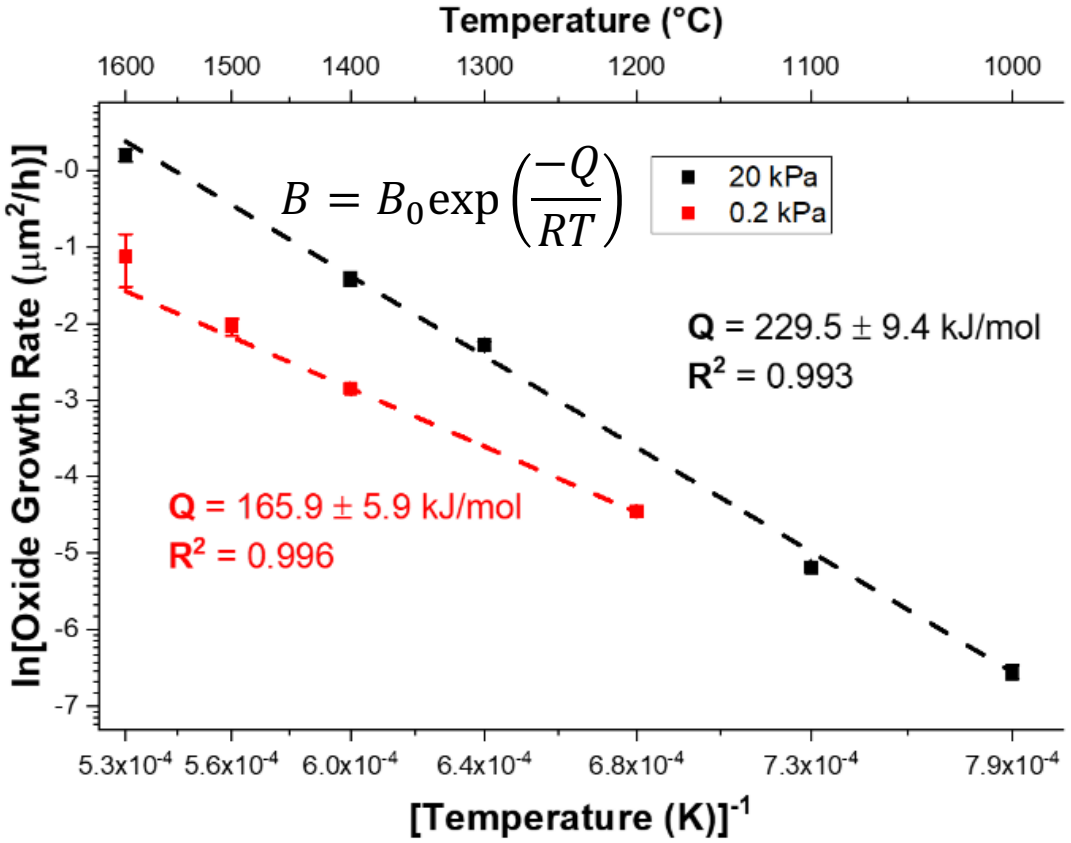

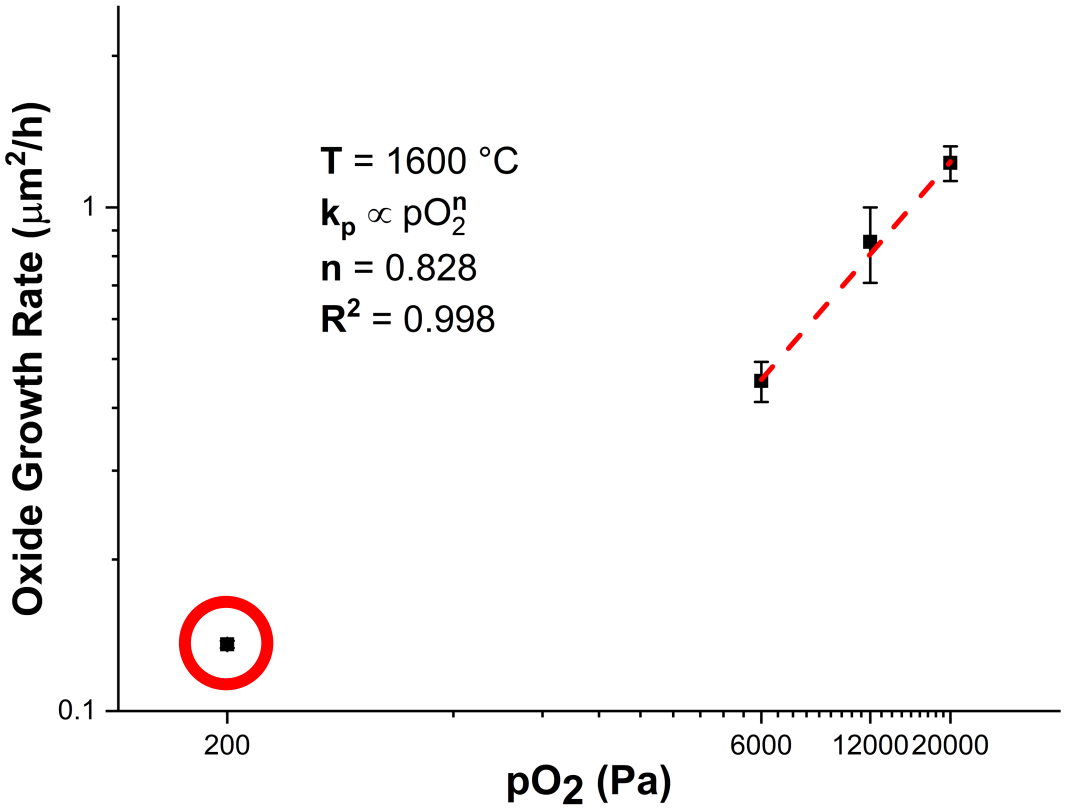

STEM Analysis of Nodules

- Crystalline SiO_2 in nodule, amorphous outside
- High number density of interfacial pores under nodules
- Crystalline nodules only above NC SiC; amorphous SiO_2 above UFG SiC

1500 °C, 0.2 kPa, 2 h

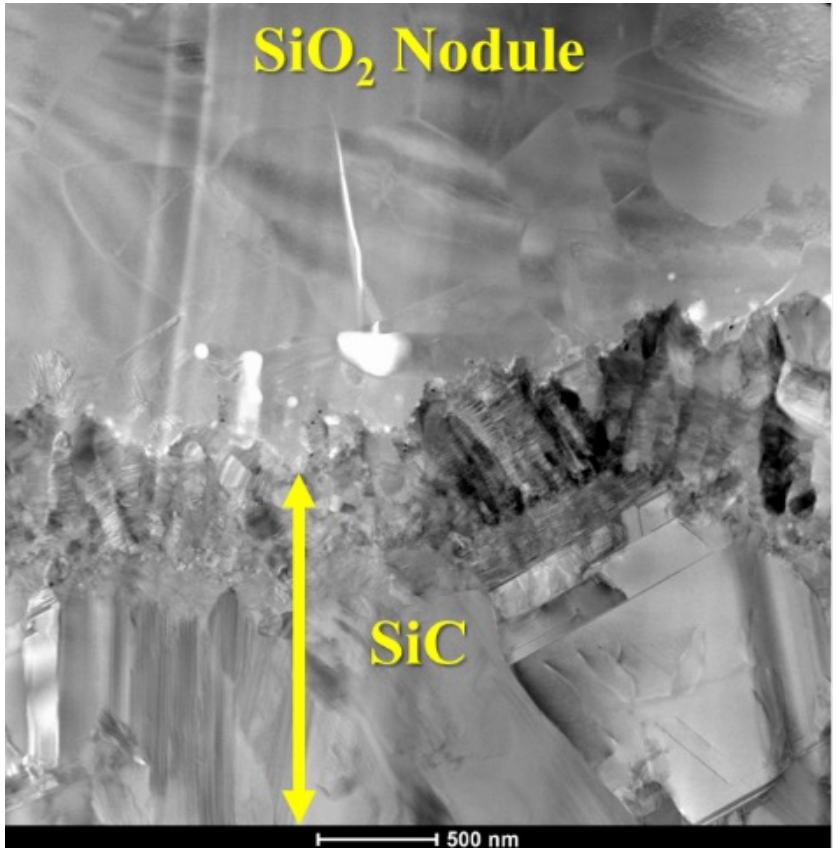

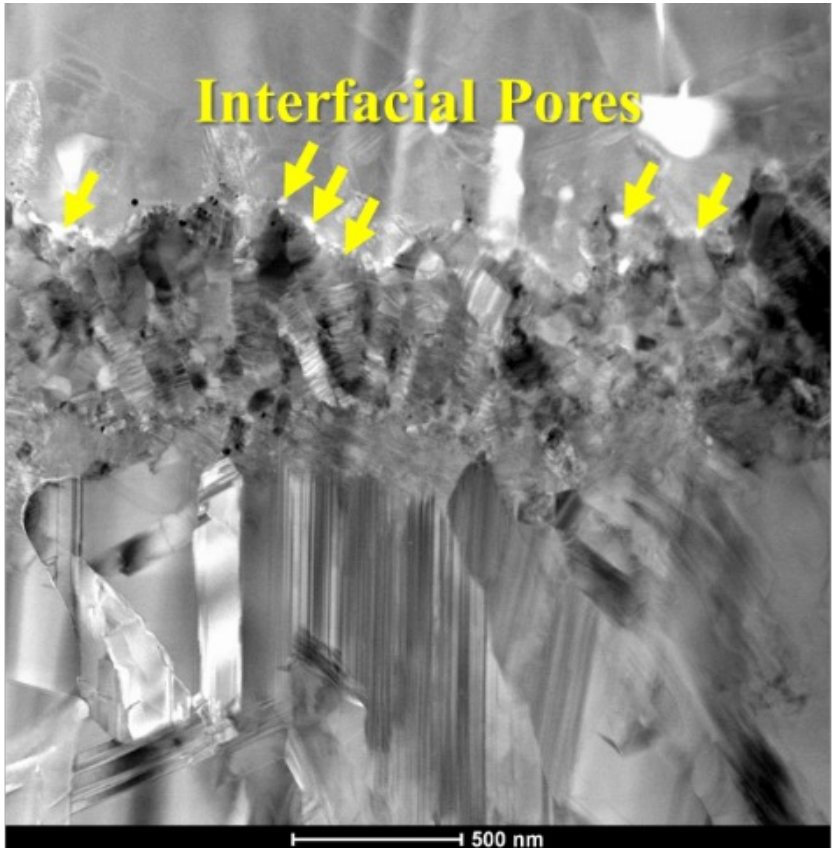

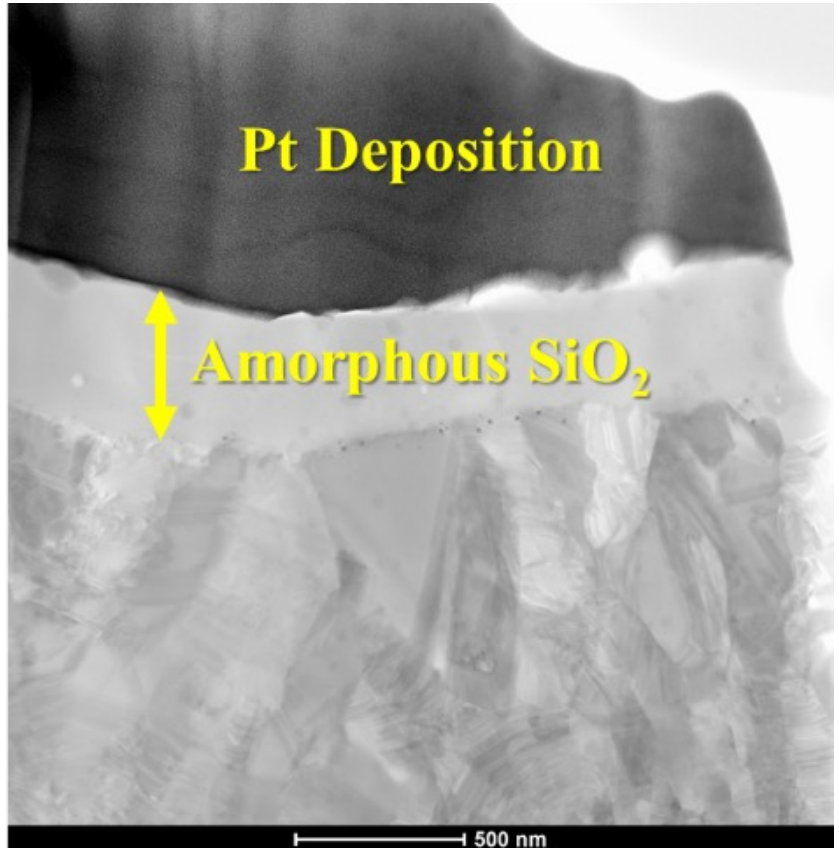

Bratten AT, Wen HM, et al., Influence of Temperature, Oxygen Partial Pressure, and Microstructure on the High-Temperature Oxidation Behavior of the SiC Layer of TRISO Particles," to be submitted to *Acta Materialia*.

APT data: Oxidation in 1300 °C Air

- Proxigram shows Si enrichment near SiO_2
- Local depletion of C near the interface
- Possible intermediate phase region ~10 nm thick
  - Actual width unknown due to interface effects

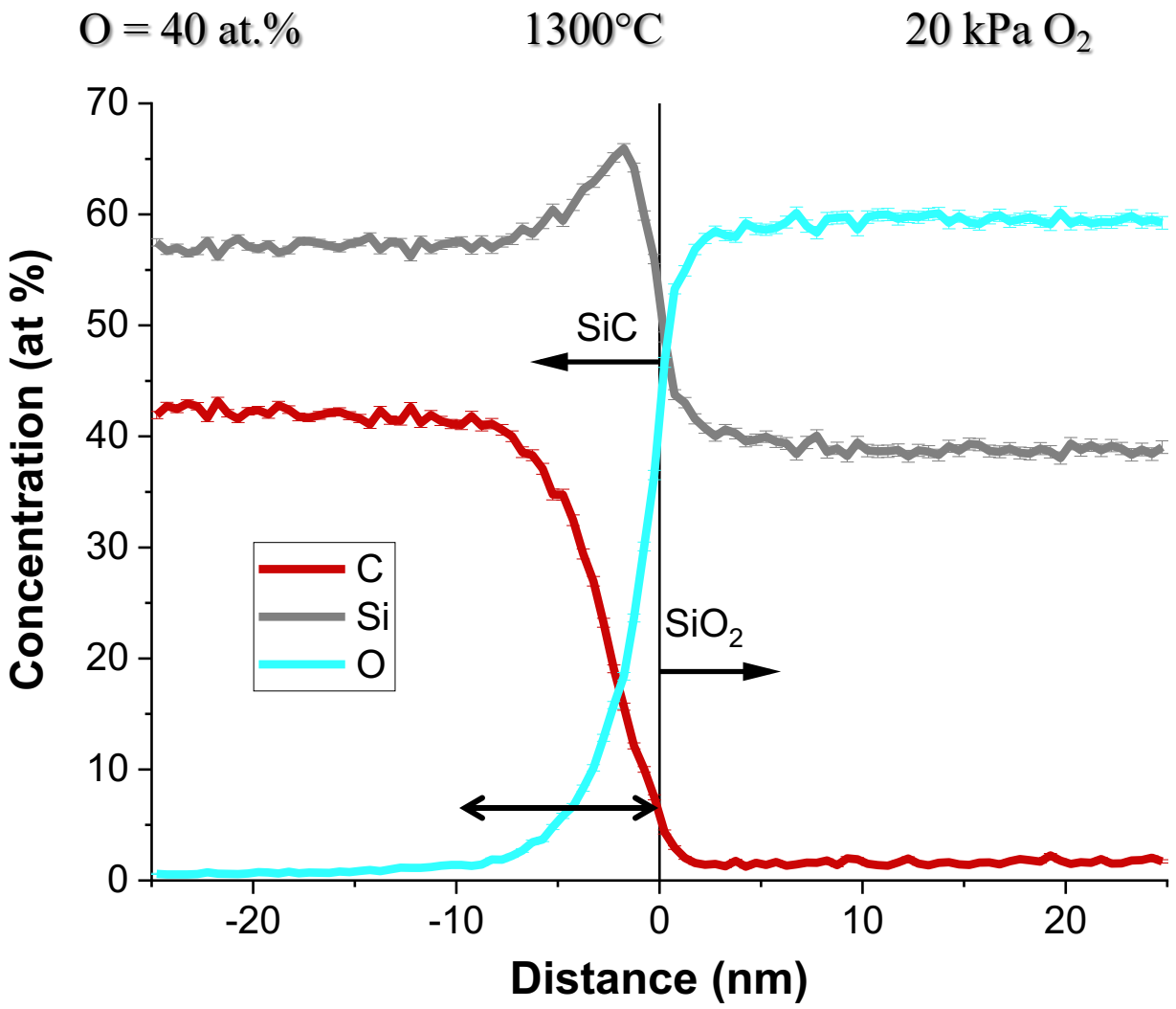

Bratten AT, Wen HM, et al., Influence of Temperature, Oxygen Partial Pressure, and Microstructure on the High-Temperature Oxidation Behavior of the SiC Layer of TRISO Particles," to be submitted to *Acta Materialia*.

APT results: Oxidation in 1600 °C, 0.2 kPa O_2

- Carbon removed from grain boundary region
- Directly correlated with oxygen penetration along GBs

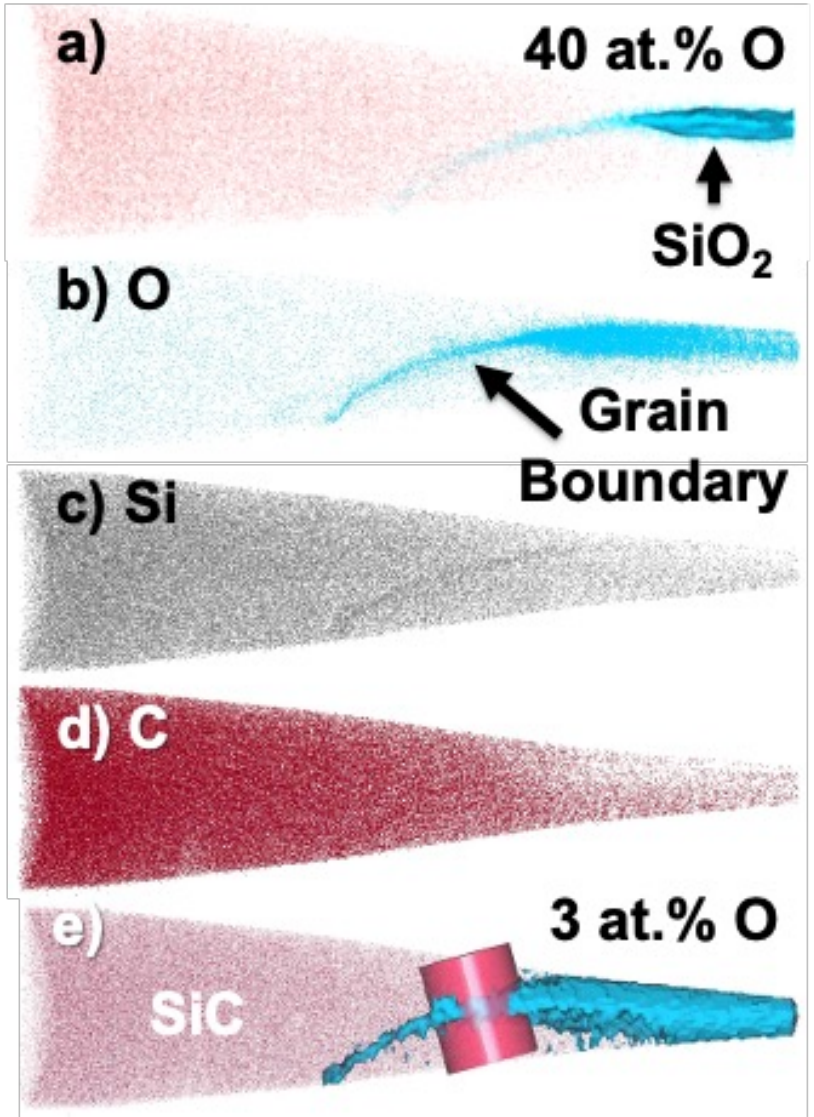

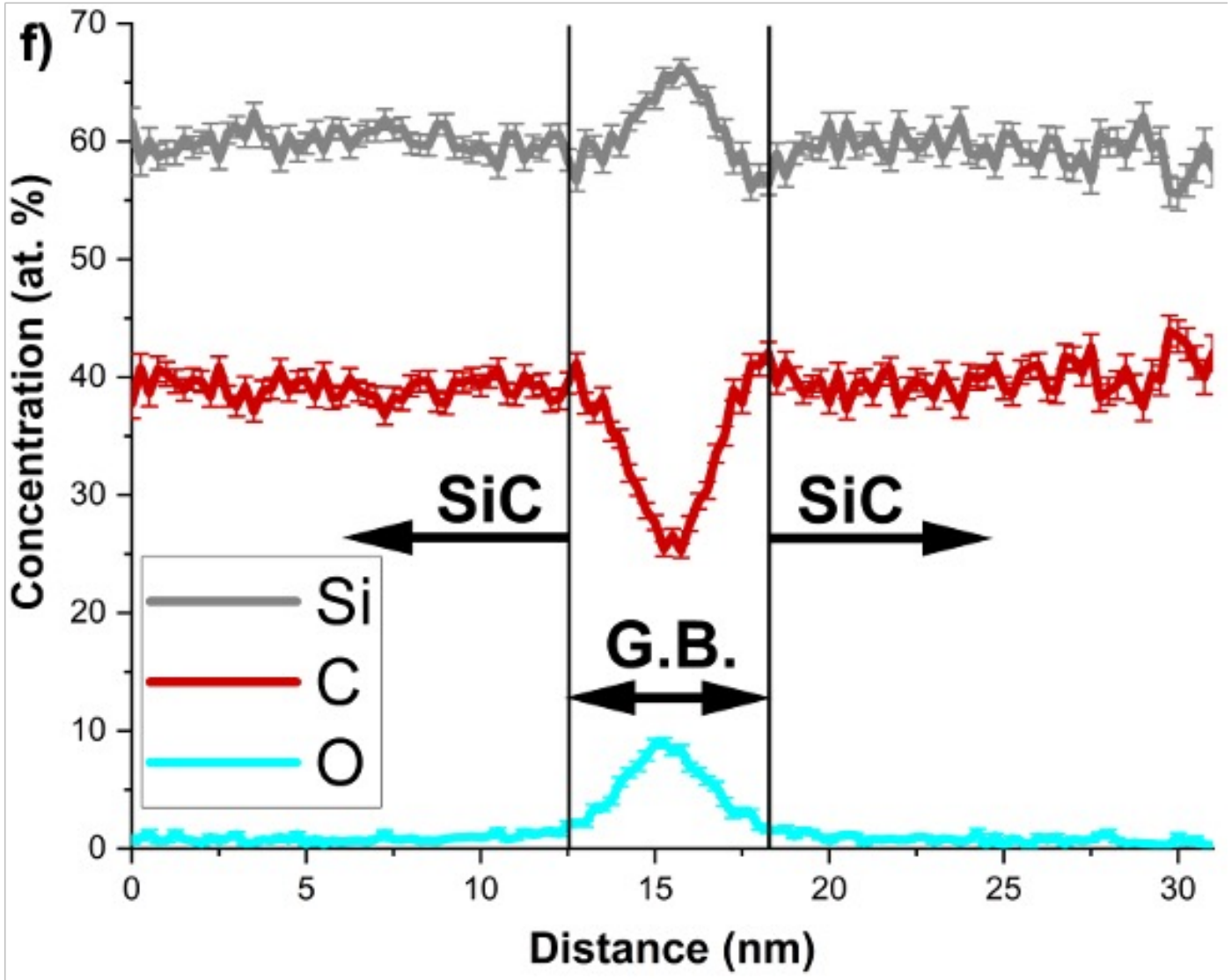

Summary: Oxidation of SiC of Surrogate TRISO Particles

- Oxidation in 20 kPa produces oxide scales with uniform thickness
  - Behavior effectively described as passive oxidation
  - Amorphous scale forms first, devitrification then occurs, producing spherulitic regions/cracks
  - Time needed for crystallization decreases with increasing temperature
  - Longer time oxidation leads to cracking of the crystalline oxide scale
- Oxidation in 0.2 kPa O_2 produces nonuniform oxide layer
  - SiC oxidation involves both passive and active oxidation
  - Nanocrystalline SiC promotes active oxidation, followed by redeposition of SiO_2 to form crystalline nodules.
  - Above ultrafine-grained SiC, only passive oxidation occurs.
- Enhanced O diffusion along grain boundaries in nanocrystalline region of SiC may cause extraction of C and formation of CO, which builds up at SiC-SiO_2 interface and promotes active oxidation, followed by redeposition of SiO_2

Acknowledgements

- The research project is financially supported by U.S. Department of Energy, through the Nuclear Energy University Program (NEUP, Award Number DE-NE0008753).
- Students working on the project: Dr. Adam Bratten, Visharad Jalan.
- APT data acquisition funded by CNMS User Proposal CNMS2021-647
- Collaborator at Idaho National Laboratory: Dr. John Stempien
- Collaborators at Oak Ridge National Laboratory: Dr. Tyler Gerczak, Dr. Jon Poplawsky
- Collaborator at University of Idaho: Prof. Haiyan Zhao

Haiming Wen Research Group at Missouri S&T